Liquid Crystal Based Label-Free Optical Sensors for Biochemical Application

Jieyuan TANG[3,4†], Zhibin LI[3,4†], Mengyuan XIE[3,4], Yunhan LUO[3,4], Jianhui YU[3,4], Guojie CHEN[1,2*], and Zhe CHEN[4,5*]

[1]*School of Physics and Optoelectronic Engineering, Foshan University, Foshan 528225, China*

[2]*Guangdong-Hong Kong-Macao Joint Laboratory for Intelligent Micro-Nano Optoelectronic Technology, Foshan University, Foshan 528225, China*

[3]*Key Laboratory of Optoelectronic Information and Sensing Technologies of Guangdong Higher Education Institutes, Jinan University, Guangzhou 510632, China*

[4]*Department of Optoelectronic Engineering, Jinan University, Guangzhou 510632, China*

[5]*JiHua Laboratory, Foshan 528200, China*

[†]*These authors contributed equally to this work and should be considered co-first authors.*

[*]Corresponding authors: Guojie CHEN and Zhe CHEN E-mail: gjchen@fosu.edu.cn and thzhechen@jnu.edu.cn

Abstract: Biochemical sensors have important applications in biology, chemistry, and medicine. Nevertheless, many biochemical sensors are hampered by intricate techniques, cumbersome procedures, and the need for labeling. In the past two decades, it has been discovered that liquid crystals can be used to achieve the optical amplification of biological interactions. By modifying recognition molecules, a variety of label-free biochemical sensors can be created. Consequently, biochemical sensors based on the amplification of liquid crystals have become one of the most promising sensors. This paper describes in detail the optical sensing principle of liquid crystals, sensing devices, and optical detection technologies. Meanwhile, the latest research findings are elucidated. Finally, the challenges and future research directions are discussed.

Keywords: Optical sensor; biochemistry; liquid crystal; label-free

Citation: Jieyuan TANG, Zhibin LI, Mengyuan XIE, Yunhan LUO, Jianhui YU, Guojie CHEN, *et al.*, "Liquid Crystal Based Label-Free Optical Sensors for Biochemical Application," *Photonic Sensors*, 2024, 14(2): 240203.

1. Introduction

Liquid crystals (LCs) are fluid with the easily-organized molecules arrangement. They have crystal-like optical properties that depend on the arrangement of LC molecules. Since the arrangement of LC molecules is very sensitive to outside influences, variations in the optical characteristics of LCs can be used to detect external stimuli. If the external stimuli are biochemical molecules or biochemical processes, LCs can be used to construct a biochemical sensor.

As early as 1964, Fergason *et al.* [1] proposed to use the change of the periodic spiral arrangement of the cholesteric liquid crystal (CLC), which could alter the color of the reflected light and detect volatile organic compounds (VOCs). The CLCs exhibit the ability to reflect particular monochromatic photons and produce vibrant color due to the helical organization of their molecules,

Received: 28 August 2023 / Revised: 23 November 2023

DOI: 10.1007/s13320-024-0707-3
Article type: Review

much to the behavior observed in gratings. More interesting, their helical arrangements are extremely susceptible to the penetration of VOCs or temperature, so they are really suitable for the VOCs or temperature detection [1–5]. In 1998, Gupta *et al*. [6] demonstrated the use of the nematic liquid crystal (NLC) film for specific biochemical sensing and proposed the concept of "LC optical amplification". The interaction of biological molecules represents a phenomenon occurring at the microscopic level, making it challenging to examine. The optical properties of LCs are plainly detectable macroscopic qualities. The optical properties of the LC at the macroscopic level are influenced by the molecular interactions occurring at the microscopic level, resulting in "optical amplification". The main principle is the disturbance of the arrangement of the NLC by the biochemical molecules interactions, which can be easily distinguished by a polarization optical microscope (POM). This label-free specific NLC sensor technology represents a milestone, as it brings a boom of research on label-free LC-based biochemical sensors [7–12].

Fluidity is the feature of LCs, which gives flexibility to the application of LCs, but at the same time, it also brings problems of the poor stability. To enhance the stability, various sensing devices were designed, such as the LC film sandwiched between two pieces of glass [13], the LC cell confined in transmission electron microscope (TEM) grid [14, 15], polymeric multilayer LC droplets [16], polymer dispersion LC [17], and LC polymer network [18, 19]. Specificity is an essential feature for biochemical sensors. In order to enhance the specificity of LC-based sensors, it is imperative to appropriately design the selective binding of recognition molecules to target molecules. Furthermore, it is crucial to consider appropriate modifications of functional groups and anchor molecules.

A viable approach to enhance the sensitivity of LC-based sensors involves augmenting the contact area between LCs and the target molecules, or combining some amplification approaches [20]. Choosing an appropriate detection technology is also an effective way. For CLCs, the color change of CLC films, which is induced by the target molecules (such as VOCs), can be detected with the naked eye or spectral technique [21]. The optical microscope image technology is commonly used to discern the texture variation of LC films or LC droplets generated by specific interactions with biological molecules in the case of NLCs [7]. In addition, some other optical technologies are used for LC sensors. Resonant wavelengths of the whispering gallery mode (WGM) of LC droplets are closely related to the refractive index of LCs. A tiny change in the arrangement of LC molecules can cause large drifts of the resonant wavelength, therefore biochemical interactions that trigger the re-arrangement of LCs can be detected [22]. Optical fibers have been used in the field of biochemical sensing due to their small size, excellent biocompatibility, corrosion resistance, and some other advantages. Micro-fabricated fiber structures, including the side polished fiber (SPF) [23], hollow fiber [24], and Mach-Zenhder interference (MZI) fiber structure [25], have the capability to detect the rearrangement of the LC. Consequently, the optical fiber sensing technology can be effectively employed for LC sensors.

This article provides an overview of the primary optical sensing properties shown by LCs, along with several sensing devices utilized in LC-based sensing applications. Subsequently, a comprehensive analysis is conducted on various optical detecting techniques that are frequently employed in LC sensors, such as the optical fiber technology, spectroscopy, surface plasmon resonance (SPR) sensing technology, and WGM sensing technology, combining with the latest practical application. In the concluding section, we discuss the difficulties encountered by LC-based sensors and the future directions of research.

2. Sensing principle of liquid crystal based optical sensors

LCs are fluid but exhibit crystal-like optical properties. The optical properties of LCs are closely related to the arrangement of LC molecules. If LC molecules are rod-shaped and the long axes of LC molecules are roughly parallel to each other, the direction of long axes is called the orientation of the LC.

According to the orientation of LCs, LCs can be classified into NLC, smectic liquid crystal (SLC), and CLC, as seen in Fig. 1. NLC molecules can travel freely, so they are extremely sensitive to their surroundings, making them ideal for sensing research. The molecules of the SLC are arranged in layers. Although molecules within the layer are allowed to move, the orientation of each layer must be roughly parallel. SLCs are infrequently used in sensors. Similar to SLCs, the molecules in CLCs are layered in layers. However, comparing with SLCs, the difference is that the orientation of the two neighboring layers undergoes an angular twist, gradually forming a spiral structure. CLCs are also frequently used to manufacture sensors. The optical properties of LCs are closely related to their orientations, therefore, different kinds of LCs have their own peculiar properties.

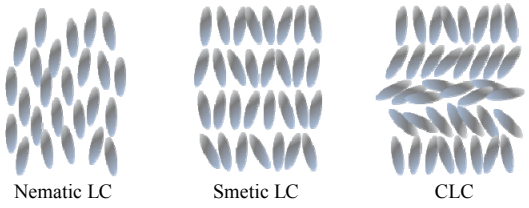

Fig. 1 Schematic of the classification of LCs.

2.1 Nematic liquid crystal

Birefringence is one of the most notable optical properties of the NLC, which is utilized in the construction of NLC sensors. As shown in Fig. 2(a), if the NLC film is oriented perpendicular to the LC interface and the incident rays penetrate it vertically, the LC film will not exhibit birefringent properties. The NLC film shows a dark field under POM. The horizontally oriented NLC film demonstrates birefringent properties. In other words, when a light beam passes through the LC film, it splits into two beams, which are known as the ordinary rays (o-rays) and extraordinary rays (e-rays), as shown in Fig. 2(b). The polarization direction of the o-rays is perpendicular to the plane of incidence, and that of the e-rays is parallel to the plane of incidence. The refractive index of o-rays (n_o) is constant. However, the refractive index of e-rays [$n_e(\theta)$] is variable, which depends on the incident angle. The refractive index of e-rays [$n_e(\theta)$] can be calculated by the following formula:

$$\frac{\sin^2\theta}{n_e^2}+\frac{\cos^2\theta}{n_o^2}=\frac{1}{n_e(\theta)} \tag{1}$$

where θ is the incident angle. n_o and n_e are both related to the wavelength of incident rays and the dielectric constant of the LC. The phase difference between the two beams is

$$\Delta\varphi=\frac{2\pi d}{\lambda}\left[n_e(\theta)-n_o\right] \tag{2}$$

where d is the thickness of the LC film, λ is the wavelength of incident rays. We may observe the colorful interference pattern under the POM because the phase difference between the two beams relies on the wavelength, the thickness of the LC film, and the incident angle. When an LC film is placed between two mutually perpendicular linear polarizers, the intensity of the transmitted light passing through the polarizers can be described by

$$I=A\sin^2\left(\frac{\Delta\varphi}{2}\right) \tag{3}$$

where A is a constant.

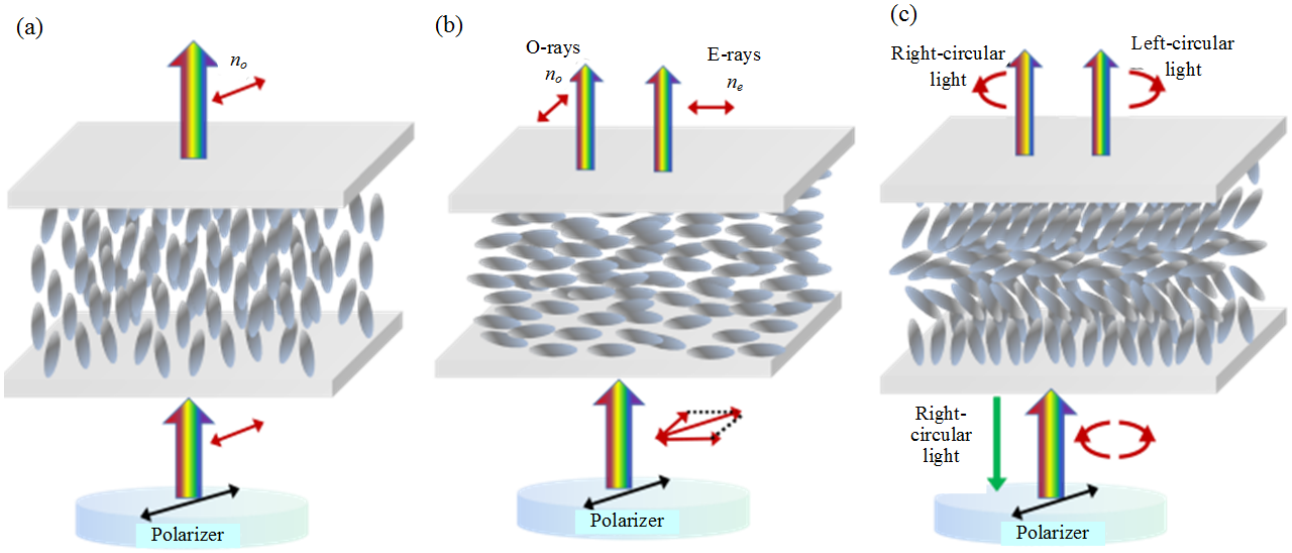

Fig. 2 Optical properties of LCs: (a) NLC with perpendicular orientation, (b) NLC with horizontal orientation, and (c) CLC.

2.2 Cholesteric liquid crystal

The earliest LCs are known as CLCs, because they are made of cholesterol derivatives. CLCs have their molecules stacked in layers. Layer by layer, the molecule's orientation is gently distorted to form a helical structure. A similar helical arrangement of LC molecules could be produced by mixing chiral dopants in NLCs. Chiral dopants have the ability to rearrange NLCs into a helical structure. Due to the similarity in the molecular arrangement between chiral NLCs and CLCs, they share optical properties such as optical rotation, selective reflection, and circular polarization dichroism, so CLCs frequently contain chiral NLCs. CLCs exhibit the optical characteristics of the grating because of the periodic structure of their molecular arrangement, which allow them to reflect light that meets the grating condition [Fig. 2(c)]. CLCs can be utilized to construct a variety of sensors by virtue of this property. For CLCs, the pitch p is the distance that the CLC molecule's orientation turns 360°, which is similar to the period in a grating. The wavelength of the reflected light satisfies

$$\lambda = mn_{\mathrm{CLC}}p \qquad (m=1, 2, 3, 4,\cdots) \qquad (4)$$

where n_{CLC} is the effective refractive index of the CLC. Unlike a grating, the reflected light from the CLC is circularly polarized in the same direction as the helical orientation of the CLC. Even if (4) is satisfied, the circularly polarized light in the opposite direction will not be reflected.

3. Liquid crystal based optical sensing devices

In the recent past, LCs have become frequently used to construct biochemical sensors. This is because the interactions between biochemical molecules can easily perturb the orientation of LCs, and these perturbances can be quickly detected by the optical features of LCs. This is also known as the amplification effect of the LC. The phrase "amplification effect of the LC" pertains to the process, by which the optical characteristics of an LC in the macroscopic realm are altered by the molecular interactions occurring in the microscopic realm. With appropriate molecular modifications, specific interactions between molecules can be detected without bio-labeling and complex processing. In response to various detection environments, numerous sensing devices, such as

LC films [6, 26, 27], LC droplets [28–30], and LC fibers [31, 32], were proposed. In this section, we elaborate on a variety of LC sensing devices, modification methods, and their biochemical application.

3.1 Sensing devices

The optical properties of an LC film will change if the external stimulus causes the LC molecules adjacent to the interface to realign over multiple micrometer distances. This is the LCs' long-range orderliness, which also serves as the foundation for the majority of LC-based sensors. Constructing an LC-based sensor must consider three aspects: 1) LCs are kept stable during the test; 2) specific interactions of the recognition and target molecules can perturb the arrangement of LCs; 3) the change in optical properties induced by the reordering of LCs can be detected.

A thin layer of the LC film, with a thickness of tens of microns, is confined between two glass slides that have been pre-modified. On one glass slide, the recognition molecules are immobilized beforehand. The interaction of the target molecules and recognition molecules occurs at the LC/solid interface, where the ordering of LC molecules is perturbed, as shown in Fig. 3(a). Since the LC film is only a few tens of microns thick, this perturbance propagates readily throughout the entire film and alters its optical properties. The LC film is confined between two glass slides, and the fluidity of the LC is well suppressed. This sandwiched LC sensing device is extremely simple to construct. Two modified glass slides are used to construct an empty LC box with the 20 μm to 30 μm thickness. The LC is heated to be an isotropic state and then pushed into the empty LC box via the siphon effect. This sensing device has been used in the sensing research of numerous biochemical materials since it is inexpensive, simple to construct, and label-free [9]. In order to simplify the fabrication process of the LC sensing device and also improve the sensitivity, Wu *et al*. [33] spin-coated an LC thin film directly on a dimethyloctadecyl [3-(trimethylsilyl)propyl] ammonium chloride (DMOAP) decorated glass slide. The film thickness can be precisely controlled by adjusting the spin rate, and decreasing the film thickness is rewarded with an increased sensitivity. The limit of detection (LOD) for bovine serum albumin (BSA) is decreased from 10^{-5} g/ml with a 4.2-μm-thick sandwiched LC device to 10^{-7} g/ml with a 4.2-μm-thick spin-coated LC film and further to 10^{-8} g/ml by reducing the LC film thickness to 3.4 μm [33].

However, numerous biochemical reactions occur in a solution and are closely related to the pH value [34, 35] and temperature [36]. Real-time monitoring of biological events occurring in a solution is not possible with the sandwiched LC sensing devices. Due to the inability of gas to pass through the glass slide, the detection of gas is similarly challenging to accomplish. The LC film with the solid base and free upper surface could be used to detect gas [37] or some biochemical reactions [33], but is not suitable to be used in a solution because the LC may be washed away. Using LC cells with a glass substrate and a TEM grid [Fig. 3(b)], a reliable LC sensing device for keeping track of biochemical activities in a solution may be built. A TEM grid LC device can be built by fixing a TEM grid to a glass slide, dropping LC into the grid, and then removing the excess LC with a capillary tube [14, 15, 26]. By selecting a suitable grid size, it is possible to effectively restrict the flow of the LC within the TEM grid and ignore the effect of the grid boundaries on the LC ordering. Of course, the LC in the TEM grid will be lost if the grid is not attached tightly to the glass slide. This issue can be avoided by fixing the LC in a section of a capillary tube [38–41] [Fig. 3(c)].

LC droplets, as shown in Fig. 3(d), have lately gained popularity as sensing devices since the time-consuming grid setting and glass slide

modification are not necessary. The LC can be dispersed in a solution by vortexing, sonication, homogenization or gentle shearing by hand [42], which constructs the simplest LC droplet sensing devices [the upper part of Fig. 3(d)]. These methods are highly straightforward and practical for detection research. However, the size of the LC droplets is inconsistent [28]. When subjected to identical anchoring conditions, micrometer-sized LC droplets display a bipolar arrangement, while nanometer-sized LC droplets exhibit a radial configuration [43]. In order to get a high level of precision, it is imperative to employ LC droplets that possess uniform sizes. This is due to the fact that LC droplets with varying sizes may manifest distinct configurations even under the same conditions [34]. An alternative approach to generate LC droplets is to dissolve the LC in an organic solvent and then drop it onto a modified solid substrate for natural evaporation [44–47]. An inkjet printer is also used to create evenly sized LC droplets on a solid material [48]. These LC droplets are generally homogeneous in size, however, they are pinned to the solid substrate and appear as LC islands (or LC hemispheres), as shown in the lower part of Fig. 3(d). Uniformly sized LC droplets can also be fabricated using silica templates and polymeric shells. Silica template particles [(8±0.2) μm] were covered in six layers of poly-4-benzenesulfonic acid sodium/polyallylamine hydrochloride (PSS/PAH) polymers by Gupta *et al*. [49]. After that, the silica cores were etched, and LC was added to the resulting capsules. Recently, an even broader approach is created by strictly controlling the flow velocities of the LC and dispersion liquid using a microchannel to produce uniformly sized LC droplets (LC spheres) [29, 50]. However, when LC droplets (LC spheres) suspend in the solution, they gradually coalesce and precipitate. Oscar *et al*. [51] employed a Pickering stabilization strategy consisting of surfactant-nanoparticle complexes that adsorbed to aqueous/LC droplet interfaces. This strategy can keep LC droplets against coalescence for at least three months. Some polymers can also promote the stability of LC droplets. Deng *et al*. [52] coated positively charged poly (diallyldimethylammonium chloride) (PDADMAC) on the negatively charged sulfated β-cyclodextrin (β-CD)/tetradecyl sulfate sodium ($SC_{14}S$) complex-engineered LC droplets through electrostatic interaction. The PDADMAC/sulfated β-CD/$SC_{14}S$ complex-coated LC droplets are highly stable in the aqueous solution and can be washed with water without changing their configurations. Hydrogel is also an excellent material for stabilizing LC droplets in the aqueous solution [53, 54]. Zhang *et al.* [53] dispersed the LC in the polyacrylamide precursor solution as emulsions, which was solidified as the hydrogel film. By embedding LC droplets in polyacrylamide hydrogel films, they overcome the problem of LC droplet sensors' poor preservation. Furthermore, hydrogel can be utilized to construct LC droplets. Liu *et al.* [55] fabricated functional LC core/hydrogel spheres for live cell monitoring using the microfluidic technology.

LC shells are an alternative device for biosensor applications. The LC shells' water-filled cores allow for the restriction of both the interior and outside surfaces [56]. Kwon *et al*. [35] fabricated LC double emulsion droplets (LC shells) using the microfluidic method, and a pH-responsive LC shell sensor had been constructed. Heo *et al.* [57] employed a microfluidic technique to fabricate solid-state NLC shell membranes. This was achieved by utilizing reactive mesogen mixture (RMM727) and 4-cyano-4'-biphenylcarbonitrile (5CB) LC, followed by ultraviolet (UV) curing and subsequent extraction of 5CB.

In addition to films and droplets, LCs can be utilized to make fibers for biochemical sensing. Wang *et al.* [58] created LC and polylactic acid (PLA) composite fibers by electrospinning a

homogeneous PLA/LC/solvent solution (7.5 wt% PLA, 11.3 wt% 5CB, 20.3 wt% acetone, and 60.9 wt% chloroform) onto cleaned glass plates. Reyes *et al.* [31, 32] proposed LC-functionalized fibers [Fig. 3(e)], which could be used to detect organic vapors. The fiber has a core made of the LC and a cladding formed by poly(vinylpyrrolidone) (PVP). The LC-functionalized fibers respond to the gas exposure with a sharp fall in brightness, and they promptly return to their former brightness when the gas is removed. Each sensing device, of course, has benefits and drawbacks. Taking into consideration, the practical use will aid in determining the most suitable type of device.

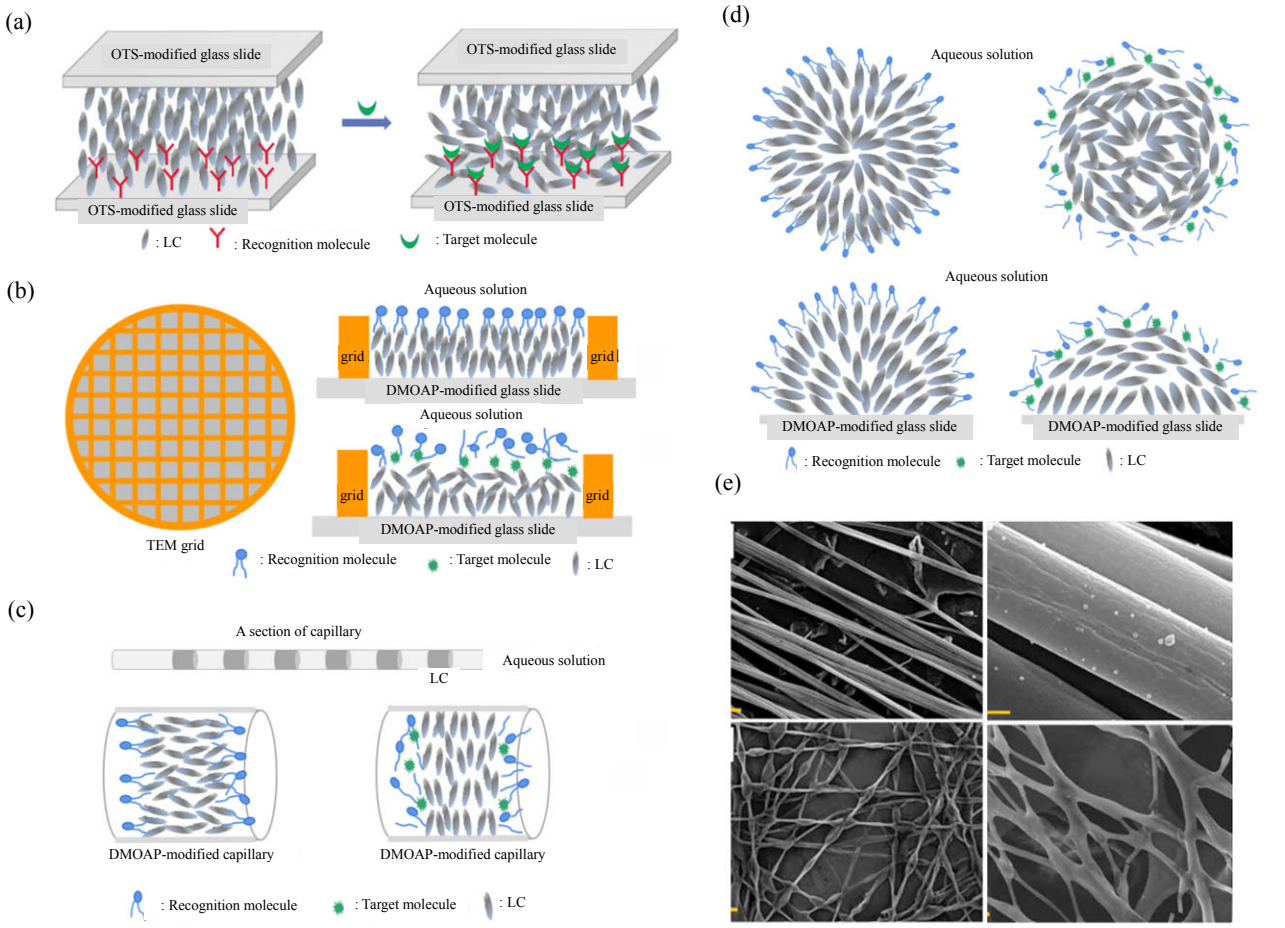

Fig. 3 Schematic illustration of LC-based sensing devices: (a) sandwich LC sensing device, (b) TEM grid LC sensing device, (c) capillary LC sensing device, (d) LC droplets sensing devices, and (e) TEM images of LC-filled PVP fibers [31].

3.2 Modification

In addition to selecting an appropriate sensing device, it is vital to consider the modification of the sensing device. To achieve the greatest change in LC optical properties when the recognition molecules capture the target molecules, we need to consider not only how to immobilize the recognition molecules, but also how to modify the anchoring molecules on the LC sensing device to achieve the desired horizontal or vertical orientation of the LC initially.

The glass slide needs to be pre-modified while making the sandwiched LC sensing devices, as discussed in the previous section. This pre-modification process includes modifying anchoring molecules and recognition molecules.

Anchoring molecules can alter the surface energy of the interface and promote regular orientation of the LC, such as perpendicular or parallel to the interface. When physically rubbing a layer of covalently bounded BSA on the surface of the glass slide, it can cause the LC to order horizontally in the direction of the mechanical rubbing at the LC/solid interface [59]. If the glass slide is coated with a gold film with nanometer-scale grooves, the LC will parallel to the surface and along the nanometer-scale grooves [60]. LC molecules are vertically aligned at the LC/solid interface by silane molecules with long alkyl tails, such as octadecyltrichlorosilane (OTS) [26] and DMOAP [61]. Due to the strong anchoring of DMOAP, the LC alignment is only disrupted by the high concentration of the target analyte. Some polymers (such as PVA) can trigger horizontal anchoring [62]. Modifying the DMOAP monolayer with PVA can generate uneven competition between the vertical and planar surface anchoring forces, and the optical response of the LC would be easier in the presence of the target analyte in the low concentration, improving the detection sensitivity [63]. The LC mixture doped by a small amount of a photocurable prepolymer, which could be used to weaken the anchoring energy of DMOAP and increase the sensitivity, is spin-coated on a glass substrate modified with DMOAP, followed by irradiation with UV light [64]. The LOD is 1.6×10^{-12} g/ml for BSA, which is much lower than that without the photocurable prepolymer [33].

In addition to modifying the anchoring molecules, it is also necessary to fix the recognition molecules at the interface. (3-aminopropyl) triethoxysilane (APTES) and glutaraldehyde (GA) are often immobilized on the solid surface to connect recognition molecules, such as DNA aptamers, which can bind to various target analytes with the high specificity and selectivity [65]. The APTES/DMOAP/GA/aptamer modified surface has been widely used in LC-based biosensors, where DMOAP is employed for LC vertical alignment and the aptamer can capture the target molecule. This specific modification method could realize the detection of various biochemical materials, such as tumor cells [65], metal ions [66], and tobramycin [67]. Some metal ions, such as Gu^{2+}, can be utilized not only as anchor molecules, but also as recognition molecules for the detection of organophosphorus gases [45, 68–70]. The homeotropic orientation of the LC (such as 5CB) at the glass surface can be triggered by the interfacial chemical interaction between the nitrile-containing LC and metal ions, however, the coordination of the metal ions with the phosphoryl group of organophosphorus gases is greater than that with the nitrile group of the LC.

At LC/aqueous interface, some amphiphiles (such as surfactant [71–73], phospholipid [74], and peptide [75]) can induce homeotropic orientation at the LC/aqueous interface. At the LC/aqueous interface, the hydrophilic ends of amphiphiles submerge in water, and the hydrophobic chains insert into the LCs. The anionic surfactant sodium dodecyl sulphate (SDS), cationic surfactants cetyltrimethylammonium bromide (CTAB) [76], octadecyl-trimethylammonium bromide (OTAB) [77], dodecyltrimethylammonium bromide (DTAB) [78], myristoylcholine chloride (Myr) [79, 80], and positively charged natural peptide poly (L-lysine) (PLL) [75] can homeotropically align the LC at the LC/aqueous interface. Once the recognition molecules with the opposite charges bind to the surfactants, the surfactants lose their ability to induce the vertical orientation of the LCs; however, when the target analytes are captured by the recognition molecules, the surfactants are released and can once again induce the vertical orientation of the LCs [76–78, 80]. Besides, if the surfactants are decomposed by the target analytes [73, 79], the homeotropic anchoring energy is weakened and the LC molecules are rearranged. Based on these

principles, a variety of biochemical molecules can be detected. Recently, Ping *et al*. [81] embedded the surfactant in hydrogel to build the LC sensor. When the gelatin hydrogel is decomposed by the target analyte trypsin, the surfactant CTAB can be released in the solution and adsorb at the aqueous/LC interface, leading to the change of the LC's orientation [81]. β-cyclodextrin (β-CD) has a hydrophilic outer surface and a hydrophobic cavity. As host molecules, they can form host-guest complexes with some kinds of surfactants (such as SDS), which prevents the surfactant from absorbing to the LC/aqueous interface. If the target analyte can decompose β-CD [82] or combine with β-CD competitively [52], causing the surfactant to be released, the orientation of the LC will change by the adsorbing of the surfactant. DNA aptamers are frequently utilized in the field of biosensors because they can capture a variety of target analytes with the excellent specificity and selectivity [65, 83, 84]. A specific class of LC-based aptamer sensors can also be created by combining charged DNA aptamers and the surfactants with the opposite charges [46, 47, 76]. The electrostatic interaction between the aptamer and the surfactant hinders the surfactant's ability to stick to the LC/aqueous interface. The surfactant is released and adsorbs at the LC/aqueous interface when the aptamer is capturing the target analyte. This process changes the LC's orientation. The major product of UV-treated 5CB is 4'-cyano-4'-biphenylcarboxylic acid (CBA), which contains a carboxylic acid terminus and is sensitive to the pH value. Due to its amphiphilic property, the deprotonated CBA (CBA^-) can self-assemble at the LC/aqueous interface, which is similar to the behavior of the surfactant or lipid [85]. 4'-pentyl-biphenyl-4-carboxylic acid (PBA) owns a similar molecular structure to CBA, therefore, PBA-doped LC is also highly sensitive to the pH value [86, 87]. The deprotonated PBA or CBA at the aqueous/LC interface can trigger configuration transitions from bipolar to radial of LC droplets [86]. As a result, the LC doped with either CBA or PBA can distinguish the biochemical processes that alter the pH value of the solution.

Polyelectrolytes (PE) are the polymers that carry ionizable groups. Polyelectrolytes can be used to modify the LC interface and construct LC-based sensors [88–91]. Bera *et al.* [89] found that the adsorption of positively charged poly (amido amine) (PAMAM) dendrimers on negatively charged poly(styrenesulfonate sodium) (PSS) coated LC droplets could trigger a bipolar-to-radial configuration transition. Yeo *et al*. [90] functionalized the LC/aqueous interface with poly(acrylic acid)-b-poly (4-cyanobiphenyl-4'-oxyundecylacrylate) (PAA-b-LCP), and the LCP block was anchored to the LC and the PAA block formed complexes with metal ions in water.

4. Optical detection technology and application

4.1 Optical microscopy

There are numerous technologies and methods for the optical detection of LCs. Polarizing imaging is the most intuitive method as LCs own the property of birefringence. The orientational transition of the LCs induced by the interactions of biochemical molecules can be observed by the POM, which was first proposed by Abbott's team [6] for biochemical sensors in 1998. This method quickly gained popularity because it does not require expensive and complicated equipment and label-free, and the results can be observed visually. With parallel illumination, the NLC film with the perpendicular orientation is dark under the POM, while the horizontal or hybrid orientation is in the bright state. The NLC films show dark/bright transition under the POM, which could help us to detect lipid-protein interaction [74], specific and non-specific protein interactions [92], ligand-receptor interaction [93], and host-guest recognition [82].

Actually, more details can be discovered by observing the NLCs' patterns and colors under the POM as they are in the process of transition. Both lipids and surfactants have the ability to induce a vertical orientation of the LC at the LC/aqueous interface, however, there are observable differences in the patterns and colors of the NLC films. Figure 4(a) displays the gradual change in color of an NLC film under POM induced by altering the concentration of the surfactant SDS solution. The colorful patterns observed in the NLC film can be attributed to its birefringent properties, while the color change is a result of variations in the orientation angle of the NLC molecules [94, 95]. When the thickness of the NLC film is determined, the Michel-Levy interference color chart [96] can be used to calculate the tilt angle of the NLC at the interface. Figure 4(b) shows the quantification of the LC tilt angle at the aqueous/LC interface in various concentrations of the SDS solution. Figure 4(c) reveals the orientational transition of the NLC film induced by phospholipid [97]. With the aid of the POM, we can see from the upper row of Fig. 4(c) that the black zone (vertical orientation area) gradually appears, enlarges from small to huge, and eventually fills the entire LC film. As shown in the lower row of Fig. 4(c), phospholipid molecules are progressively adsorbed to the LC interface during this procedure. These findings show that both the phospholipids and surfactants can induce the vertical orientation of LCs, but their actions on LC molecules are very different. By contrasting the LC patterns, Devi *et al*. [74] discovered that two distinct phospholipid-modified LC films displayed discrepancies with respect to the same cytoplasmic protein. Figure 4(d) shows the polarization optical responses of LCs at different phospholipid-based LC interfaces [1, 2-dilauroyl-snglycero-3-phosphocholine (DLPC) and lysophosphatidic acid (LPA)] to cytoplasmic protein [juxtamembrane of epidermal growth factor receptor (JM-EGFR)]. Elongated brilliant domains are seen at a DLPC-laden interface, whereas an LPA-laden interface shows a uniform bright texture. The formation of distinctly shaped optical domains of LCs is probably associated with the different secondary structures adopted by the JM-EGFR protein.

Due to the internal hybrid arrangements of LC molecules, the polarization images of LC droplets are intricate. LC droplets can be categorized as LC islands (LC hemispheres), LC spheres, and LC shells. Even in the same external environment, different types of LC droplets show distinct optical patterns under the POM. For the LC islands (sessile droplets), whose solid interface is vertically anchored, dark-cross to windmill (four-clover) patterns can be visible when the orientation at the LC/aqueous interface shifts from the radial to tangential, as shown in Fig. 4(e) [48]. In the case of LC spheres, monodisperse LC spheres suspend in the solution and go through an ordering transition from the bipolar to radial forms when the concentration of SDS increases, as shown in Fig. 4(f) [49]. Bipolar director-configured LC spheres often align tangential to the surface contour. In the related bright-field or polarized light micrograph, there is a round brilliant spot with two diametrically opposed point defects (called boojums) at the LC sphere's poles. The radial director structure is characterized by a solitary point defect located at the center of the LC sphere, which can be observed using the bright-field light microscope. A cross like pattern (or Maltese cross pattern) is visible in the polarized light micrograph [49].

The configurations of the LC shells are more complicated because both the inner and outer interfaces can be oriented, and the LC shells' polarized light micrographs contain more patterns. Figure 4(g) depicts four distinct director configurations: P/P, H/H, P/H, and H/P (H represents homeotropic and P represents planar), with the microscope's focal planes located at the 1) top, 2) midsection, and 3) bottom of the LC shells [35].

Perhaps due to the complexity of LC shells preparation, their application as the biochemical sensor is uncommon. Table 1 shows the latest application of NLC-based biochemical sensors of the optical microscopy.

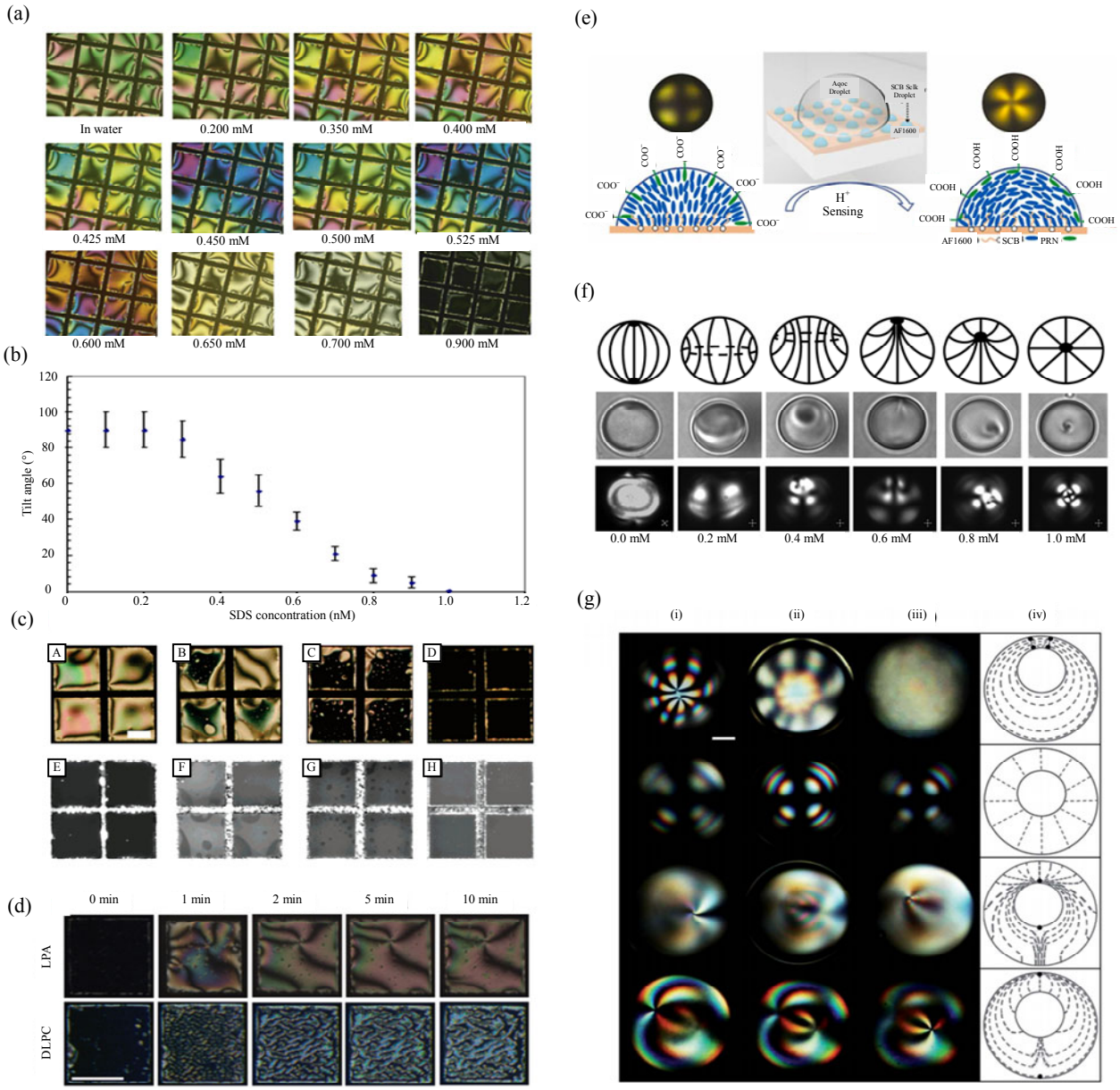

Fig. 4 Optical microscopic images of different types of NLC-based sensing devices: (a) polarized light micrographs of 5CB in the SDS solution, (b) quantification of the tilt angle of the LC at the aqueous/5CB interface [94], (c) polarized light micrographs (the upper row) and corresponding epifluorescence micrographs (the lower row) of 5CB during the transfer of phospholipid L-DLPC (0.1 mM) to the aqueous/LC interface in the TBS solution [97], (d) polarized optical response of LPA or DLPC laden LC film upon the addition of JM-EGFR (300 nM) at different time intervals [74], (e) configuration changes of LC islands are corresponding to the interfacial molecular alignment induced by deprotonated PBA (radial) and protonated PBA (tangential) [48], (f) surface-driven ordering transitions in polymer-encapsulated LC droplets in the SDS solutions ranging from 0 mM to 1 mM. The central and bottom rows, respectively, display the equivalent bright-field and polarized light micrographs of the 5CB droplets, whereas the top row schematically illustrates the topological ordering of the LC within each droplet [49], and (g) POM images and topological ordering for functionalized NLC shells with four different configurations [35].

Table 1 NLC-based biochemical sensing application of optical microscopy.

Sensing device	Target	Recognition molecule	Principle	LOD	Ref.
Sandwiched 5CB film	Kanamycin	DNA aptamer	AuNPs-Kana-aptamer conjugates can destroy the arrangement of the LC film	0.1 pM	[84]
Sandwiched 5CB film	Amoxicillin (AMX)	DNA aptamer	The specific binding of the aptamer and AMX disrupts the homeotropic orientation of the LC film	3.5 nM	[83]
Sandwiched 5CB film	Cecropin B (CB)	Anti-CB	The specific binding of CB and anti-CB results in the change of the arrangement of the LC film	1.49×10^{-2} ng/ml	[98]
Sandwiched 5CB film	Protein kinase C (PKC)	Anti-PKC	The specific binding of PKC and anti-PKC results in the change of the arrangement of the LC film	1.680±0.005 ng/ml	[99]
Sandwiched E7 film	Circulating tumor cell	DNA aptamer	Specific binding between the EpCAM-specific aptamer and EpCAM-postive cells can destroy the arrangement of the LC film	5 cells	[65]
Microcapillary confined 5CB	α-amylase	β-CD/ SDS	The degradation of β-CD in the host-guest inclusion complex by α-amylase releases SDS molecules and facilitates a change in the LC orientation	100 ng/ml	[40]
Rectangular capillaries confined 5CB	Anti-human serum albumin (anti-HSA)	Human serum albumin (HSA)	The specific binding between HSA and anti-HSA disrupts the original orientation of the LC	1 μg/ml	[41]
Spin-coated E7 film or HDN film	Cancer biomarker CA125 antigen	Anti-CA125	Alignment of LC molecules is disrupted due to the formation of the CA125 immune complexes	10^{-5} g/ml (E7); 10^{-8} g/ml (HDN)	[33]
TEM grid 5CB film	Malathion	DNA aptamer and CTAB	CTAB-aptamer interactions are diminished by the formation of aptamer-malathion complexes, which releases CTAB and changes the LC orientation	0.465 nM	[27]
TEM grid 5CB film	JM-EGFR protein	DLPC	DLPC self-assembling on the LC surface is disrupted by the adsorption of JM-EGFR protein	50 nM	[74]
TEM grid 5CB film	Ibuprofen	DNA aptamer and CTAB	When the aptamer captures target ibuprofen, CTAB will be released and change the orientation of the LC	12.5 μg/ml	[76]
TEM grid OTAB-doped 5CB film	Thrombin	DNA aptamer	The interaction between the thrombin and aptamer disrupts the electrostatic interaction between aptamer and OTAB, which releases OTAB	~ 136 nM	[80]
TEM grid OTAB-doped 5CB film	Tumor Markers CEA, PSA, and AFP	Probe DNA	Magnetic bead is coated with an aptamer 1, target tumor marker, and aptamer 2, and then releases signal DNA, which is recognized by the DNA-laden LC sensor	0.31 ng/ml (CEA); 0.07 ng/ml (PSA); 0.19 ng/ml (AFP)	[100]
TEM grid OTAB-doped 5CB film	Uric acid (UA) and uricase (UOx)	OTAB	The ssDNA is released by the UOx-catalyzed oxidation of UA. The interaction of the ssDNA and OTAB disrupt the OTAB monolayer at the aqueous/5CB interface	0.001 μM (UA); 0.34 μg/ml (UOx)	[101]
TEM grid dodecyloxyurea -doped 5CB film	Copper ions	Oxyurea	Dodecyloxyurea aligns the LC, which is disrupted by the complexation of dodecyloxyurea and Cu^{2+} ion	10 μM	[102]
5CB droplets (spheres)	Cholic acid (CA)	SDS	Competitive reaction of CA at the SDS-laden 5CB droplet surface induces the configuration transition of the LC	5 μM	[28]
E7 droplets (spheres)	Antimicrobial peptides Smp43	Phospholipid	Smp43 (an α-helical peptide) exhibits membrane disruptive activity against phospholipid, inducing the configuration transition of the LC	0.9 μM	[29]
5CB droplets (spheres)	Endotoxin	-	Interactions of endotoxin with topological defects are induced by the geometry of the LC droplets.	~1 pg/ml	[30]
5CB droplets (spheres)	Deoxycholic acid (DCA), CA	Sulfate β-CD	Bile acids can displace the $SC_{14}S$ from the cavity of the sulfate β-CD immobilized at the surface of the 5CB droplets	2 μM (DCA); 20 μM (CA)	[52]
5CB droplets (spheres)	BSA, concanavalin A (ConA), cathepsinD (CathD)	Cationic poly (L-lysine) (PLL)	Electrostatic interactions between the protein and cationic PLL trigger a quick transition in the director configuration of the LC droplets	0.1 μg/ml (BSA); 50 μg/ml (ConA); 250 μg/ml (CathD)	[75]
5CB droplets (islands)	Carboxylesterase	Myristoylcholine chloride	Carboxylesterase can catalyze the hydrolysis of myristoylcholine chloride, triggering a transition in the director configuration of the LC	0.1 mg/L	[44]
5CB droplets (islands)	Organophosphate nerve (DMMP)	Cu $(ClO_4)_2$	The stronger coordination interaction of Cu $(ClO_4)_2$ with DMMP than that with 5CB triggers the orientational transition of the LC	2.0 ppb	[45]
5CB droplets (islands)	Kanamycin	DNA aptamer	The specific binding of kanamycin to its aptamer can release the CTAB and trigger the orientational transition of the LC	0.1 ng/ml	[46]
5CB droplets (islands)	Aflatoxin B1	DNA aptamer	The specific binding of aflatoxin B1 to its aptamer can release the CTAB and trigger the orientational transition of the LC	10 pg/ml	[47]
PBA-doped 5CB droplets (islands)	Penicillin G	Penicillinase	PBA-doped 5CB droplets are sensitive to the pH value, which can be altered by penicillinase's enzymatic hydrolysis	0.178 ng/ml	[48]
Hydrogel stabilized LC droplets	Adenosine triphosphate (ATP)	Arginine (Arg.)	The interaction between the guanidine groups on Arg and the phosphate group on ATP can release CTAB and lead LC droplets to convert the configuration	1 ng/ml	[53]

The sensing devices made of CLCs, such as CLC films or CLC droplets, exhibit a significant difference in patterns under the POM. By examining the patterns and brightness of CLC films under the POM, Shemirani *et al*. [103] created a handheld sensor for the detection of methanol in two different alcoholic beverages. Figure 5(a) shows that the pattern of the CLC film is brightly colored and contains interference fringes covered by some oily streaks defects under the POM, regardless of whether the LC orientation at the interface is vertical or horizontal. Since the optical patterns of CLC films are harder to differentiate than those of NLCs, the polarized light microscopy is not frequently used as a detection method by CLC-film-based sensors.

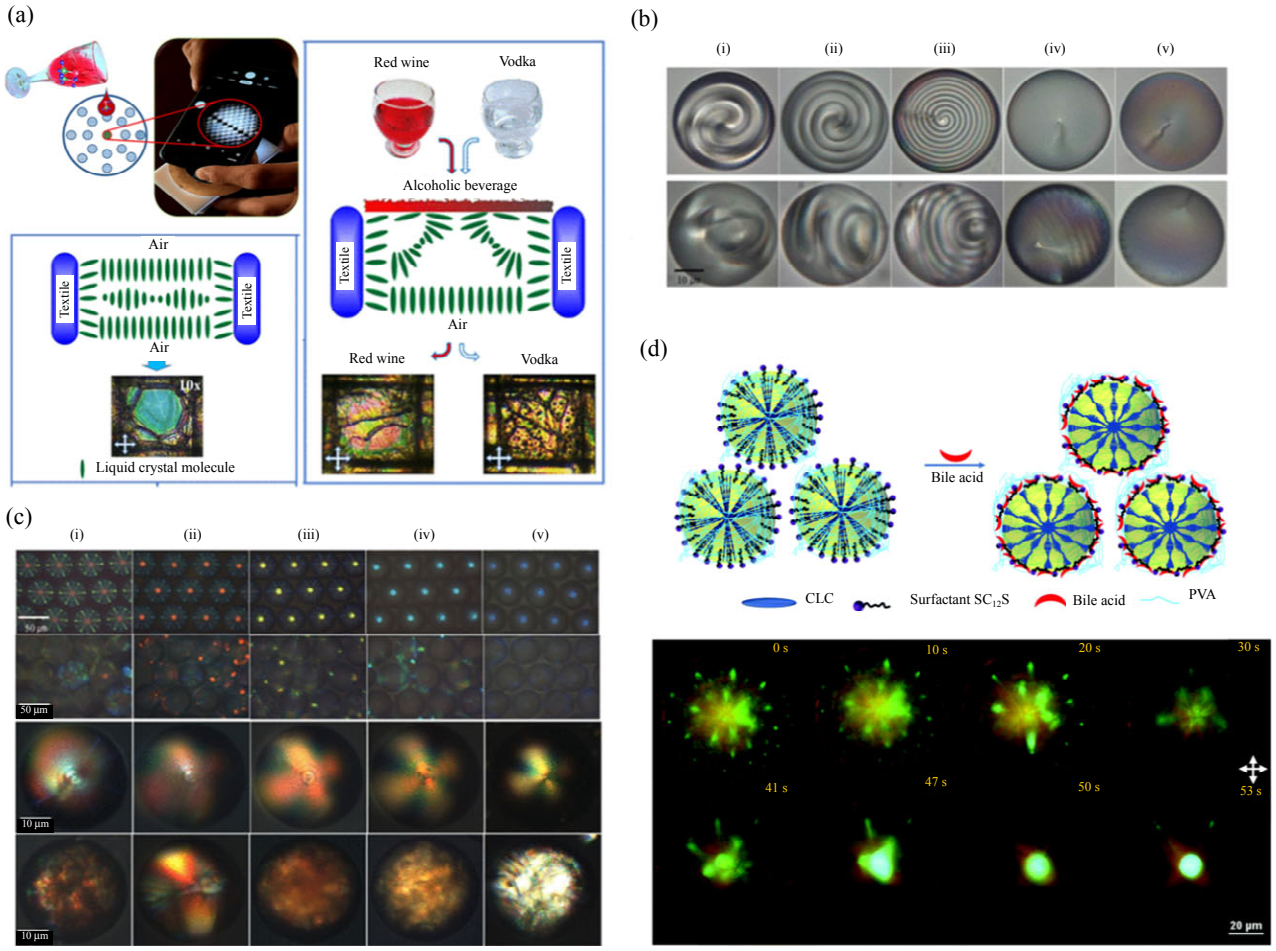

Fig. 5 Optical microscopic images of different types of CLC-based sensing devices: (a) schematic illustration of the hand-held sensor (upper left), and the corresponding polarizing micrographs when the top and bottom of the CLC film are surrounded with air (lower left) and after adding the mixture of alcoholic beverages at the CLC top surface (right) [103]; (b) bright-field transmittance mode images of CLC_{PVA} (top row) and CLC_{SDS} (bottom row) droplets with (i) 0.8 wt%, (ii) 1 wt%, (iii) 2 wt%, (iv) 5 wt%, and (v) 10 wt% chiral dopants [105]; (c) bright-field reflection-mode (the first and second rows) and polarizing transmission-mode (the third and fourth rows) of CLC_{PVA} (the first and third rows) and CLC_{SDS} (the second and fourth rows) droplets at (i) 30 wt%, (ii) 35 wt%, (iii) 40 wt%, (iv) 45 wt%, and (v) 50 wt% chiral dopants [105]; (d) schematic illustration (top) and the corresponding polarizing micrographs (bottom) of the director configuration transition of PVA/$SC_{12}S$-stabilized CLC droplets from homeotropic to planar, which is triggered by $SC_{12}S$-bile acid interactions at the surface of the dispersed CLC droplets (top) [106].

Due to the unique patterns of CLC droplets under the POM, there have been more and more reports of CLC droplet biosensors in recent years. The optical patterns and director configurations of CLC droplets are related to their chirality. Zhou *et al*. [104] found that, with increasing chirality, a continuous transition of CLC droplets was observed from a twisted bipolar structure to a radial spherical

structure. Lee *et al*. [105] studied the colorful patterns of low and high chiral dopant CLC droplets with the optical microscopy, with or without the crossed polarizers. For low chiral dopant CLC_{PVA} droplets (tangential orientation at the interface), helical structures with concentric rings are present [the upper row of Fig. 5(b)]. Under the homeotropic anchoring condition (CLC_{SDS}), the symmetric concentric ring structure cannot be obtained [the lower row of Fig. 5(b)]. For high chiral dopant CLC droplets, the reflection mode bright field images show different color spots at the center of the CLC_{PVA} droplets [the first row of Fig. 5(c)], depending on the concentration of the chiral dopant. For the CLC_{SDS} droplets (homeotropic orientation at the interface), strong flash light-like spots are observed [the second row of Fig. 5(c)]. Under the POM, the CLC_{PVA} droplets show a cross pattern and a series of concentric rings around a small cross pattern at the center [the third row of Fig. 5(c)], and the CLC_{SDS} droplets show irregular patterns [the fourth row of Fig. 5(c)]. Therefore, whether in the bright field or polarizing mode, with the high or low chiral dopant, the images of the CLC droplets demonstrate a significant variation with the reorientation of CLC molecules. Gollapelli *et al*. [106] reported a bile acids biosensor based on PVA/$SC_{12}S$-stabilized CLC droplets. The competing adsorption of bile acids at the surface of the CLC droplets triggers homeotropic to planar transition at the interface of the CLC droplets. Using a POM in reflection mode, the homeotropic orientation of the CLC droplets reveals flash light dots. After the addition of deoxycholic acid (DCA), these flashlight spots migrate to the center, where they turn into a large green reflection spot when the orientation of the CLC droplet becomes planar [Fig. 5(d)].

A majority of the LC-based sensors detect biochemical reactions by analyzing the average brightness or pattern of the LCs under the POM. Although the outcomes are intuitive, they are not accurate enough and vary greatly between individuals. More reliable results will be obtained by statistically analyzing a large number of polarized images. The machine learning (ML) framework can classify and analyze thousands of images that are collected during the LC responses, and the sensing accuracy is much higher than those of the traditional LC sensors [107, 108]. Bao *et al*. [109] employed a three-dimensional convolutional neural network to extract feature information encoded in the spatiotemporal color patterns of the LCs to detect O_3 and Cl_2. Esmailpour *et al*. [110] fabricated a textile grid LC sensing device for the detection of the SARS-CoV-2 virus in nasopharyngeal swab samples. The ML technique was employed to analyze LC patterns, which could distinguish negative and positive COVID-19 samples with a 96% degree of accuracy and distinguish COVID-19 samples from influenza types A and B with a 93% degree of accuracy. Using deep convolutional neural networks (CNNs) as pattern recognition systems, Frazo *et al*. [111] analyzed the dynamics of the optical textures of LC droplets in distinct VOCs. With the aid of CNNs, a single individual droplet can recognize 11 VOCs. Cao *et al.* [112] utilized Alexnet to characterize optical LC responses and spatial features, achieving 99.9% classification accuracy. However, achieving such high levels of accuracy necessitates an extremely large number of features, resulting in computational difficulties and obscuring the physical interpretability of the dominant features. In order to resolve these issues, Smith *et al*. [113] investigated the efficacy of features derived from color micrographs using visual geometry group 16 (VGG16), which might minimize the number of features to less than 100.

Some researchers integrate the LC sensing technology with the signal amplification technology to increase the sensitivity. Gold nanoparticles (AuNPs) can be used for the signal amplification in LC-based biochemical sensors [84, 98, 99]. The addition of AuNPs may amplify the disruption of the LC caused by the association of the target molecule

with the capture probe. Su *et al*. [98] immobilized the AuNPs and anti-cecropin B antibody (anti-CB) complex on the solid surface of the LC film to detect cecropin B (CB). Due to the fact that the volume of AuNPs is significantly greater than those of CB and anti-CB, AuNPs can serve as signal amplifiers, and the LOD is as low as 1.49×10^{-2} ng/ml [98]. Liu *et al*. [99] utilized the same amplification technology to detect protein kinase C (PKC), substituting the PKC antibody for an anti-CB antibody. The LOD of protein kinase C is (1.68±0.005) ng/ml. Wang *et al*. [84] reported a self-oriented beacon LC biosensor for the kanamycin detection with AuNPs signal amplification. The LOD of kanamycin is 0.1 pM, which is considerably lower than that without AuNPs signal enhancement (0.17 nM [46]). Additionally, the sensitivity can also be increased by combining the LC sensor technology and rolling circle amplification (RCA). Qi *et al*. [114] used the LC sensor to detect cancer biomarkers by employing in situ RCA on magnetic beads (MBs). Specific recognition of cancer biomarkers by aptamers results in the formation of nucleic acid circles on MBs pre-assembled with ligation DNA, linear padlock DNA, and aptamers, thereby activating in-situ RCA and altering the orientation of OTAB-decorated LC. It achieves a sensitivity enhancement of at least four orders of magnitude. Using the same amplification technique, trace quantities of lead ions can be detected, with an LOD as low as 16.7 pM [115].

4.2 Chromogenic and spectral technology

The CLC has a helical orientation and a reflection band in its spectrum, which are both affected by its refractive index and pitch. Any external stimulus that alters pitch or refractive index of the CLC, such as temperature [116, 117] or VOCs [2, 117], can cause the shift of the reflection band, which might be exploited to create CLC-based sensors. The color change can be seen with the naked eye if the reflection band is in the visible light range. This is the most intriguing aspect of CLCs. However, the visual resolution is low, and it is hard to analyze quantitatively. It is more accurate if the color shift is quantitatively examined using a computer. Avsar *et al*. [118] synthesized polymeric particles using CLCs as the template. They quantified the response of polymeric particles to the toluene vapor by analyzing the red, green, and blue average intensities of the collected images of polymeric particles.

The detection of CLCs' colors is limited by the visible light range. The spectroscopy can compensate for this limitation by collecting and analyzing a wider range of optical data, resulting in the improved precision and measuring range. CLCs are typically fabricated as thin films with molecules arranged horizontally at the interface to facilitate the detection of reflection spectra. Chang *et al*. [21] utilized the CLC film's reflection spectrum to monitor the toluene and acetone's natural volatilization. The CLC pitch increases as the organic gas permeates the CLC film, causing a red-shift of the reflected wavelength. The minimum detection limits for toluene and acetone are 48 ppm and 28.7 ppm, respectively [21]. CLCs have a good response to VOCs. However, the response depends on the composition of the CLCs, as CLCs with different compositions have distinct functional groups and polarities. Kek *et al.* [119] discovered that the reflected wavelength of CLC mixtures containing the Demus ester, Shiff base, tolan derivatives, or phenylcyclohexyl derivatives blue-shifted, when exposed to VOCs. However, without the inclusion of recognition molecules, the specific response of organic gases by CLCs is subpar. To increase the specificity and sensitivity of CLC-based sensors, it is necessary to integrate functional groups or recognition molecules that can respond to the target analyte. Sutarlie *et al*. [120] used the reflected wavelength of the dodecylamine-doped CLC to detect aldehyde vapors, The LOD for pentyl aldehyde was 2.77 ppmv and the sensitivity was 0.185 nm/ppmv.

Once an LC-based sensor is used in practice, its steadiness becomes an important factor. To enhance the stability, Sutarlie *et al*. [121] combined the CLC with the UV glue (NOA61) to make a polymer-stabilized CLC (PSCLC) for detecting vaporous amines. The UV glue (NOA61) generates a scaffold after UV curing, which may impede the flow of the CLC. The cholesteryl derivatives of the CLC can establish hydrogen bonds with the primary amine functional groups of vaporous amines, changing the color and reflected wavelength. In PSCLC, however, only the polymer is solidified, while the CLC remains fluid. CLC polymer (CLCP), which could make entirely stable solid-state LC sensors, is proposed. The CLC mixture consists of reactive mesogens (RM) for the CLC matrix, a reactive or unreactive chiral dopant, and a photoinitiator for initiating the photopolymerization procedure. To obtain the complete solid-state CLC structure, the unreactive chiral dopant or monomers must be extracted following photopolymerization. The removed portion leaves an empty region, which may be filled by a functional monomer or functional groups for sensing purposes. Chang *et al*. [18,19] proposed a hydrogen-bridged CLCP network to distinguish alcohol. During polymerization, two monoacrylates containing carboxylic acid in the CLCP network generate hydrogen bridges. Then, the hydrogen bridges are disrupted, promoting the absorption of alcohol molecules with hydrogen bonds. Following that, Yeh *et al*. [122] altered the CLCP network's composition, optimized the activation time of alkaline solution treatment, and increased the reversibility. Moirangthem *et al*. [123] fabricated a CLCP film containing benzoic acid metal binding sites, which showed the high selectivity for calcium ions. Ca^{2+} binding leads to a significant decrease in the length of the helical pitch, which may be related to the dehydration of the film, resulting in the polymer shrinkage. The blue-shift occurs in the film's reflection band. To achieve the whole solid-state structure for the CLCP film, the unreactive chiral dopant or monomer should be removed to leave the empty space. If functional network polymers are used to fill the empty space, an interpenetrated polymer network (IPN) structure is created. Stumpel *et al*. [124] created an interpenetrated CLC/hydrogel polymer network (CLC-hydrogel-IPN) to offer a humidity and pH response, using interwoven poly (acrylic acid) to cover the removed empty space. After a change in the humidity or pH value, the volume change in the hydrogel polymer causes a pitch change in the cholesteric network, resulting in a shift in the reflected wavelength. To employ CLC-hydrogel-IPN in biosensors, it is necessary to immobilize the receptor groups. Noh *et al*. [125] filled the extracted space of the CLCP film with polyacrylic acid (PAA) mixed with a cross-linker of tri (propylene glycol) diacrylate, UV-cured with a photomask to obtain a patterned array-dot film, and then functionalized the individual dots with the urease. The particles of the CLC-hydrogel-IPN array respond independently to the urea with the high sensitivity and stability via a color change and reflected wavelength. Since the reflected color and wavelength of the CLC film are highly dependent on the detection angle, the results will vary when gathering the reflected signals from various angles. Lim *et al*. [126] proposed photonic spheres to resolve this issue. As CLC molecules on the surface of the sphere are parallel to the surface, the reflected color and wavelength are unaffected by the observer's viewing angle.

Optical fibers are good waveguide media to transmit and collect optical signals. Yang *et al*. [127] used a 2×2 multimode fiber coupler to transmit the emitted light and collect the reflected light from the CLC films, which were coated at the end of the two output fibers [Fig. 6(a)]. Since the CLC films at the two ends of the fiber coupler have different compositions, the reflected wavelengths and sensitivities of the two probes to the organic gas are distinct. This dual-probe fiber CLC sensor can distinguish the concentrations of acetone and

ethanol in a mixed gas. Su *et al*. [128] made a fiber structure to detect alcohol. Two CLC droplets were placed in a hollow capillary tube that was joined by a multimode fiber for the excitation and reception of the CLC droplets' reflection spectrum [Fig. 6(b)]. The two droplets have different CLC components and reflected wavelengths. The sensitivities of the two CLC droplets are 0.296 nm/v% and 0.467 nm/v% for methanol, and 0.764 nm/v% and 1.133 nm/v% for ethanol, respectively. Li *et al.* [2] found that some PCLCs' reflected wavelengths shows a bidirectional shift as the VOC concentration rises. The difficult issue is, however, resolved by a pre-compressed process that removes some of the CLC from the PCLC films. They attach a PCLC film to the fiber's tip and utilize it to excite and capture the reflected spectrum. The sensitivity of acetone is increased to 0.23 pm/ppm after photopolymerization and sucking off a portion of the CLC. Table 2 shows the latest application of CLC-based biochemical sensors of the spectral technology.

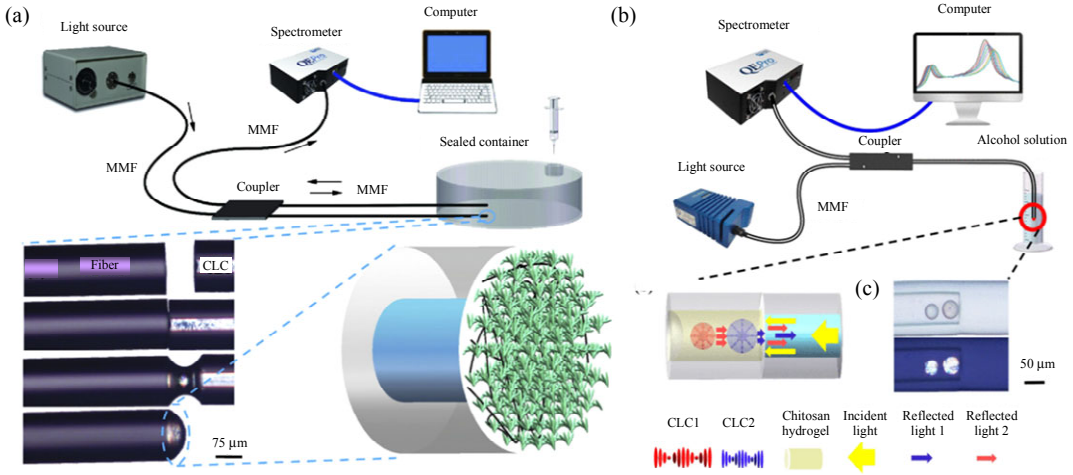

Fig. 6 CLC-based biochemical sensing application of the spectral technology: (a) setup (top) and the micro-sensing probe with the CLC film (below) [127] and (b) setup (top) and CLC droplets fiber-optic probe (below) [128].

Table 2 CLC-based biochemical sensing application of the spectral technology.

Sensing device	Target	Principle	LOD or Range	Ref.
CLC film	Toluene and acetone	The helical structure of CLC is diffused to isotropic by molecules of the organic vapor	48 ppm (toluene); 28.7 ppm(acetone)	[21]
Dodecylamine-doped CLC film	Aldehyde vapors	The primary amine group of dodecylamine can react with an aldehyde group and shorten the effective pitch of the CLCs	2.77 ppmv (pentyl aldehyde); 4.99 ppmv (butyl aldehyde); 85.02 ppmv (methyl aldehyde)	[120]
Polymer-stabilized CLC film	Decylamine	The primary amine groups of vaporous amines can form hydrogen bonds with cholesteryl derivatives of the CLC, resulting in a change in color and refracted wavelength of the CLC	2 ppmv	[121]
Chiral imprinted CLC polymer film	Calcium	The binding of Ca^{2+} results in a decrease in the helical pitch due to dehydration of the film	10^{-4} –10^{-2} M	[123]
Interpenetrated CLC/hydrogel polymer network film	Humidity	The volume change in the hydrogel polymer causes a pitch change in the cholesteric network	6%–90%	[124]
Urease-immobilized CLC-hydrogel-IPN array-dots	Urea	The enzymatic reaction of the urease with the urea produces ammonia, leading to an increase in the pH value and a change in the pitch of the cholesteric network	7.5×10^{-3} M	[125]
$CLC_{solid\text{-}IPN\text{-}urease}$ ball	Urea	The enzymatic reaction of the urease with the urea produces ammonia, leading to an increase in the pH value and a change in the pitch of the cholesteric network	1.52 mM	[126]
$CLC_{solid\text{-}IPN\text{-}KOH}$ ball	Calcium ion	The $CLC_{solid\text{-}IPN\text{-}KOH}$ contains $COO^{-}K^{+}$ complexes. Ca^{2+} can replace the K^{+} and form a bridging $-COO-Ca-COO-$ structure, thereby decreasing the pitch of the CLC	0.09 mM	[126]

The chemical bonds or functional groups of organic molecules vibrate at the infrared band. Therefore, when organic molecules are irradiated with infrared light, the energy can be absorbed by the chemical bonds or functional groups. Some LC-based biosensors rely on the competitive combination of target and recognition molecules with LC or amphiphile molecules that induce LC reorientation. The infrared absorption spectroscopy can help identify such competitive binding, thereby revealing the underlying mechanisms of LC sensing. Cadwell *et al*. [129] made use of the Fourier transform polarization modulation infrared reflection-absorption spectroscopy to reveal the influence of DMMP on the nitrile-containing LCs that are supported onto the surfaces with immobilized metal perchlorate salts. The infrared spectroscopy can elucidate the molecular origin of macroscopic ordering transitions in LCs.

4.3 Whispering gallery mode sensing technology

In a microcavity with a circular symmetry structure [Fig. 7(a)], the interference enhancement occurs when successive reflections happen as the light propagates along the inner wall and the optical path is an integer multiple of the wavelength. The modes that satisfy the condition for the interference enhancement are called WGMs, which are optical eigenmodes in the microcavity with the circular symmetry. The resonant frequency of the WGM is determined by the effective refraction index of the microcavity and optical path. Any change in the microcavity's refractive index or size can be reflected in the WGM spectrum, so WGMs could be used to fabricate sensors [130, 131].

In 2011, Humar *et al*. [132] first lased the WGM resonance in LC droplets. Millimolar SDS can alter the orientation of LC droplets, which can be detected by the WGM lasing spectrum, then the LC-WGM biochemical sensor could be constructed. Wang *et al*. [131] developed an LC droplet WGM micro-laser for ultrasensitive detection of the BSA with an LOD of 0.3 pM. Duan *et al*. [22] used stearic acid-doped LC droplets as optical micro-resonators to detect metal ions. The shift of the WGM resonant wavelength is triggered by the interaction between metal ion and deprotonated stearic acid. The LOD is as low as 40 pM for Cu(II). They also monitored the enzymatic reaction of the urease [133, 134], acetylcholinesterase, and its inhibitors [135] with the same method and technology. Figure 7(c) shows the experimental setup and the WGM lasing spectra of the 5CB droplet of the different orientations. The proposed sensor has an LOD of 0.1 mM for urea [134], 0.1 pg/ml for fenobucarb, and 1 pg/ml for dimethoate [135]. In order to capture the WGM lasing spectrum, it is crucial to fix the LC droplets when they are in an aqueous solution. Ma *et al*. [136] fabricated a fiber structure to hold an LC droplet for the salmon sperm DNA detection [Fig. 7(b)]. An LC droplet is immobilized in a hollow capillary tube, and a multimode fiber is used to transmit excited light and acquire WGM lasing signals. The sensor head can detect with just 3 nL of the sample and has an LOD of 1.32 μg/ml.

In addition to LC droplets, LC cylinders could also be used to trigger WGMs. Duan *et al*. [139] attached the glycerol trioleate (GT)-doped LC to microfiber in order to create a micro-resonator for triggering WGM lasing spectra for the lipase detection [Fig. 7(d)]. Oleic acid is created by the enzymatic reaction between lipase and GT, which causes the reorientation of the LC from planar to homeotropic. The WGM wavelength shift can be utilized to detect the LC reorientation, and the LOD of lipase is 0.01 g/ml. Using the same microfiber sensor technology, hydrogen peroxide and catalase are detected [140].

Dye molecules are usually doped into LCs for the WGM lasing. In actuality, the WGM can also be activated in the LC without dye molecules being

added. Wang *et al*. [141] created a micro-bubble structure, and then modified the inner wall with DMOAP and BSA before filling the LC without the dye. The micro-bubble structure provides a stable and reliable WGM resonator for the LC with a high Q factor. The orientation of the LC is disturbed by the immobilized BSA molecules through the reduction of the vertical anchoring force from the alignment layer. An LOD of 1 fM for the BSA is achieved, which is lower than those in their early research work [133]. Table 3 shows the latest application of LC-based biochemical sensors of the WGM.

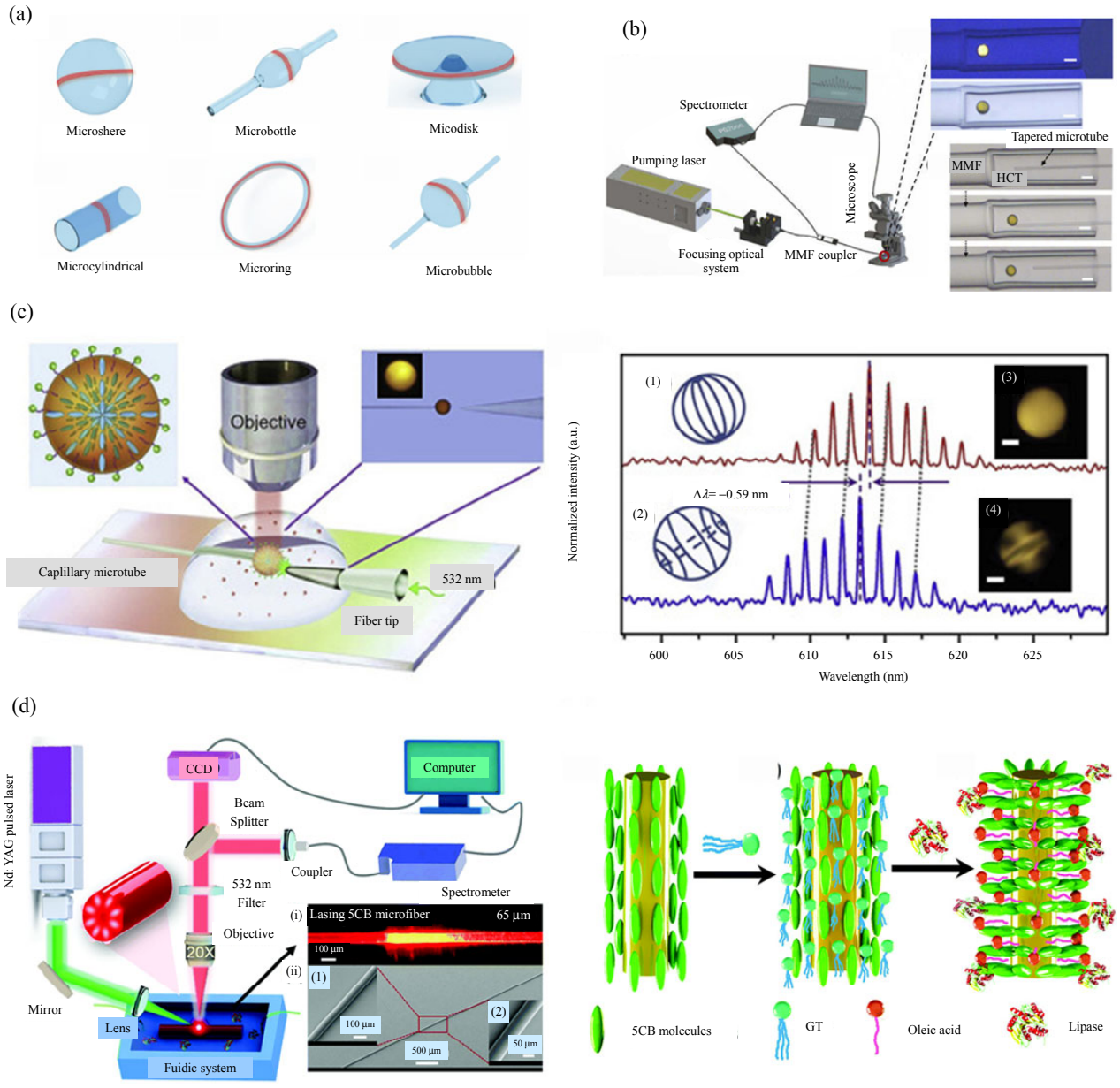

Fig. 7 LC-based biochemical sensing application of the WGM: (a) schematic diagrams of some WGM coupling structures [132], (b) schematic diagram of the experimental setup and micrograph of the probe 5CB microdroplet [138], (c) schematic diagram of the WGM lasing experimental setup with a 5 CB microdroplet at a fiber tip (left), and differently oriented 5CB microdroplet WGM lasing spectra (right) [136], and (d) schematic diagram of the experimental setup of an LC microfiber biosensor (left), and the orientation change of the LC from planar to homeotropic by the enzymatic reaction between lipase and GT (top right) [139].

Table 3 LC-based biochemical sensing application of the WGM.

Sensing device	Target	Principle	LOD or range	Ref.
Poly-L-lysine (PLL) coated 5CB droplets	BSA	The electrostatic interaction of the BSA and the PLL triggers the change of orientation, leading to the shift of WGM lasing spectra	0.36 pM	[131]
Stearic acid-doped 5CB droplets	Cu(II)	The shift of the WGM laser resonant wavelength is triggered by the interaction between metal ion and deprotonated stearic acid	40 pM	[22]
UV-treated 5CB droplets	Urease	The LC configuration transition induces the wavelength shift in WGM lasing spectra by the catalytic hydrolysis of the urea with the urease	0.5 μg/ml	[133]
Stearic acid-doped LC droplets	Urea	The enzymatic reaction between the urea and urease produces hydroxide ions, inducing the reorientation of the LC and the shift of WGM lasing spectra	0.1 mM	[134]
Myristoylcholine chloride (Myr)-coated 5CB droplets	Acetylcholine sterase (AchE) and its inhibitors	The enzymatic hydrolysis of Myr by AchE triggers the reorientation of the LC and the shift of WGM lasing spectra, but AchE's inhibitors prevent the hydrolysis process and the shift of WGM lasing spectra	1 pg/ml (dimethoate); 0.1 pg/ml (fenobucarb)	[135]
DTAB-coated 5CB droplets	Salmon sperm DNA	The DNA can absorb DTAB due to electrostatic interaction, inducing the reorientation of the LC and the shift of WGM lasing spectra	1.32 μg/ml	[136]
Glycerol trioleate (GT)-doped LC microfiber	Lipase	Oleic acid is created by the enzymatic reaction between lipase and GT, causing the reorientation of the LC and shift of WGM lasing spectra	0.01 g/ml	[137]
Dodecanal-doped LC microfiber	Hydrogen peroxide (H_2O_2) and catalase	Dodecanal can be oxidized to dodecanoic acids by H_2O_2. Dodecanoic acids can trigger reorientation of LC and shift of WGM lasing spectra. Catalase can decompose H_2O_2 and block the process above	0.26 μM (H_2O_2); 1 ng/ml (catalase)	[138]

4.4 SPR sensing technology

The SPR is the oscillation of charge density at the interface between the metal and dielectric material. In 1902, the SPR was first observed [140]. Exciting the SPR must satisfy: 1) the incident light must be TM-polarized; 2) the metal interface must be present; 3) the oscillating frequency and wave vector of the SPR along the direction of the metal interface must match those of the exciting wave. Otto [141] proposed a prism structure to realize the SPR by attenuating the total reflection, and Kretschmann [142] improved this structure to make it easier to implement. This prim structure consists of three layers [Fig. 8(a)]. The first layer is a prism (the refractive index is higher than that of the sensing layer) and the second layer is a thin metal film (gold or silver is the best). The third layer is responsible for biochemical sensing. A laser beam with TM polarization illuminates one aspect of the prism. Total reflection takes place at the prism/metal interface, where the attenuated wave travels through the metal layer and the upper sensing layer interface. If the wave vector of the attenuated wave matches with that of the surface plasmon wave, the energy of the incident laser can couple to the surface plasmon wave, and the energy of the reflected light will be drastically reduced. The wave vector of the surface plasmon wave is dependent on the dielectric constant of the sensing layer, which can be altered by the specific biochemical interactions. The SPR has played an important role in the biological and chemical sensing applications over the past two decades [143–145].

LCs are dielectric materials. When the LC film is placed on a metal surface and the refractive index of the prism is greater than that of the LC, the LC-based SPR signal can be observed. The orientation transition can alter the effective refractive index of the LC, allowing the construction of LC-SPR biochemical sensors. Vahedi *et al*. [146] simulated an LC-SPR biosensor, and the optimal structural parameters were provided in order to facilitate the experimental construction of the sensor. Although some theoretical papers on LC-SPR sensors have been published [146–149] and their feasibility has been confirmed, there have only been a few experimental findings.

Kieser *et al*. fabricated an LC-SPR sensor for the

sensing of VOCs and temperature [150]. A phase transition from a nematic to an isotropic state takes place at the VOC percolation in the LC film, changing the LC's effective refractive index and the SPR wavelength [150]. Although the experimental feasibility of the LC-SPR has been demonstrated, the sensing device lacks the specificity. According to Abbott' researches, the adsorbate-induced ordering transitions of the LCs on the surfaces of the nanodots could be characterized using the localized surface plasmon resonances (LSPRs) of gold nanodots submerged under LCs [Fig. 8(b)] [151]. The copper carboxylate-functionalized nanodots were covered with a 10 μm thick layer of 5CB. The LSPR response caused by the binding of DMMP to Cu^{2+} at the nanodots' surfaces was detected, and the LSPR wavelength blue-shifted by 1.7 nm for every 10 ppm DMMP [151].

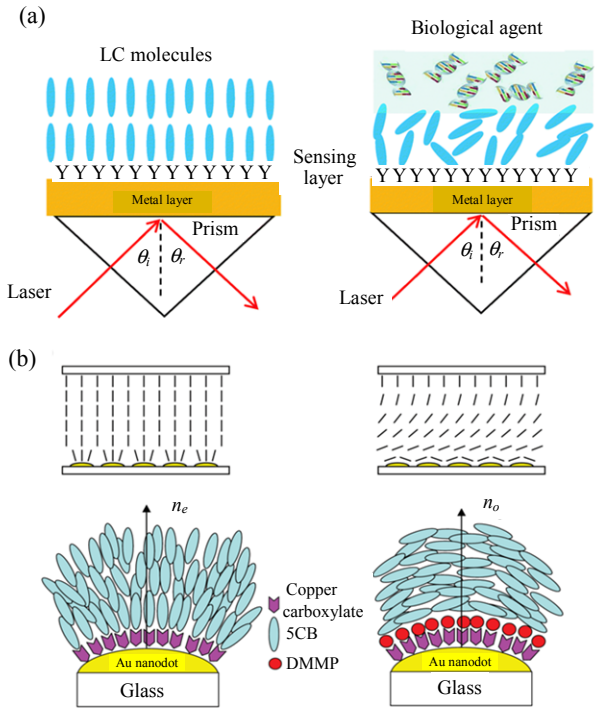

Fig. 8 Sensing principles of the SPR-LC sensors: (a) typical SPR-LC sensor with the Kretschmann configuration [147] and (b) schematic diagram of using the localized SPR to probe the adsorbate-driven ordering transitions of LCs in contact with chemically functionalized gold nanodots [151].

4.5 Optical fiber sensing technology

Optical fiber sensors offer a prospective alternative platform for implementing biological sensors due to their unique advantages, including their small size, immunity to electromagnetic interference, biocompatibility, and quick response. There are many types of optical fiber sensors, such as optical fiber grating [152], fiber SPR [153], Sagnac interferometer [154], evanescent wave sensor [155], Mach-Zehnder interferometer [156], Fabry-Perot interferometer [157, 158], lossy mode resonance [159], and surface-enhanced Raman scattering [160]. Most fiber sensors are based on the changes in the environmental refractive index induced by the interaction of biochemical molecules. However, a majority of biological reactions take place in the solution, which has a low refractive index of 1.33 and limits the sensitivity in fiber optic sensors. To enhance the sensitivity of the fiber sensor, a sensitive material is added. Recently, researchers found that LCs are also an effective sensitive medium for optical fiber sensors [23, 161].

4.5.1 Evanescent wave optical fiber sensor

Various optical fiber structures for biochemical sensors have been reported. The side-polished fiber (SPF) has significant advantages over other fiber structures in terms of fabrication ease, mechanical strength, and cost. The transmitted optical power can leak from the side-polished region of the fiber to generate an evanescent field that interacts with the external environment, and its D-shaped cross section makes it possible to construct a flat platform onto which sensitive materials can be readily integrated. Tang *et al.* [23] proposed a biosensor based on an SPF, onto which LC and phospholipid are integrated. The left schematic diagram of Fig. 9(a) shows the setup and the principle of the LC-based SPF sensor for the phospholipase A_2 (PLA_2) detection. The SPF is modified with DMOAP and then coated with the LC. The LC-coated SPF is then self-assembled the phospholipid recognition molecules. This process of self-assembly induces the LC dewetting, which

ultimately results in polar oriented LC droplets. When the solution contains the target molecule PLA_2, the hydrolysis of phospholipid by PLA_2 triggers the realignment and morphological transformation of LC droplets on the SPF, which not only alters the effective refractive index of the LC but also induces the change of the transmitted light power of the fiber sensor, as depicted by the right curve in Fig. 9(a). The proposed fiber sensor has a low LOD (1 nM) and offers the possibility of being incorporated into micro-flow processors to quantitatively detect biological molecules in real time and online. Tang *et al*. [162] also coated the CLC film on the surface of a side polished fiber, the wavelength selectively coupling from the SPF's evanescent field to the CLC film results in the resonant dips in the transmitted spectrum, as seen in Fig. 9(b). The refractive index of the LC decreases with increasing VOC concentration and results in a blue-shift of the resonance dip.

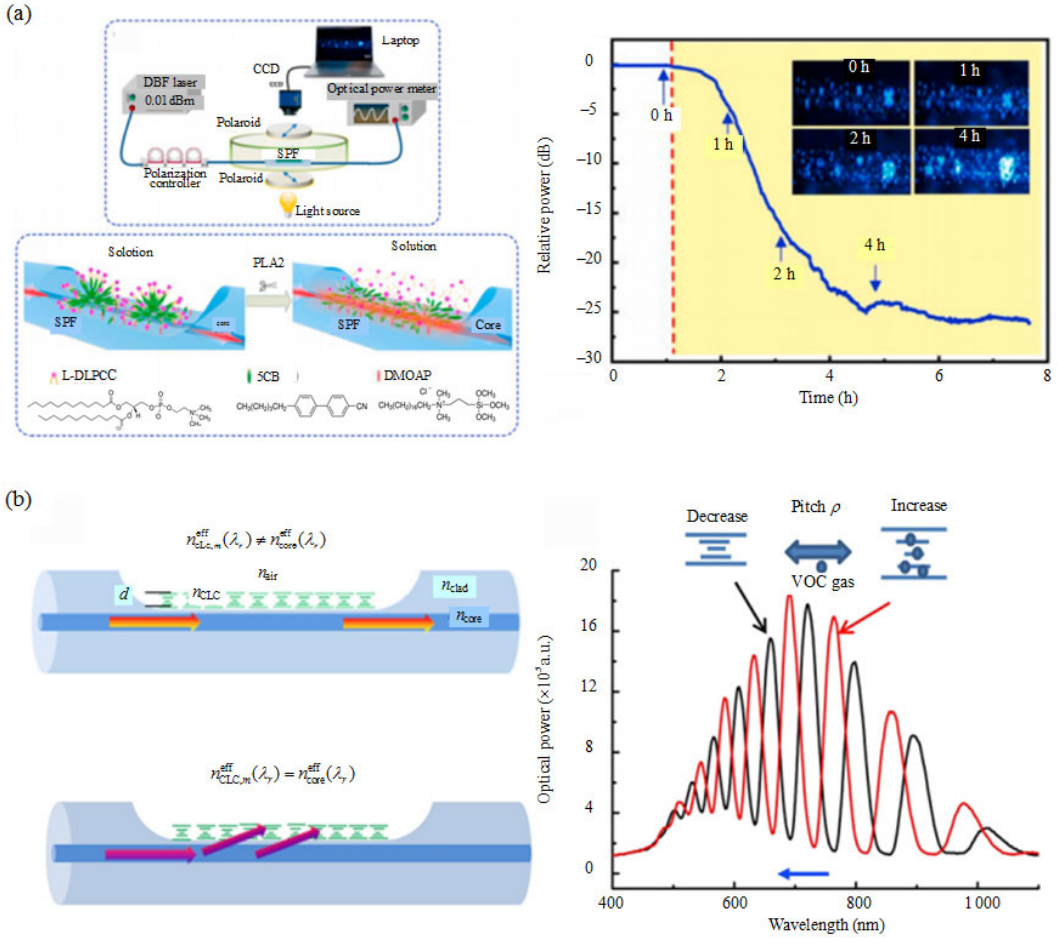

Fig. 9 LC-based evanescent wave optical fiber sensing application: (a) experimental setup and principle of the LC-based SPF fiber sensor for the PLA_2 detection (left); variation in the transmission intensity of the LC-coated SPF when detecting PLA_2 (right) [23]; (b) schematic illustration of the change in the CLC pitch and light coupling between the CLC film and the SPF (left); the transmitted spectra for the CLCFC-SPF unexposed (black line) and exposed (red line) to volatile gas (right) [162].

4.5.2 MZI

Li *et al*. [24] fabricated a fiber MZI based on LCs for the VOC vapor detection [Fig. 10(a)]. The MZI fiber structure consists of two single-mode fibers and one microtubule. The side of the microtubule is grooved using femtosecond laser. The LC is stuffed into the crevice. The sensitivities of 83 pm/ppm, 31 pm/ppm, and 101.4 pm/ppm

correspond to vapors of methanol, acetone, and ethanol, respectively. Hu *et al*. [25] proposed an LC biosensor, based on an optical fiber MZI [Fig. 10(b)]. The optical fiber-based MZI structure is composed of two single-mode fibers and a tapered photonic crystal fiber (PCF). The PCF is coated with the PBA-doped LC. The PBA can reorder LC molecules according to the ambient pH value, which changes the refractive index of the LC and realizes a sensor sensitivity to the pH value of 1.2nm/pH. The enzymatic reaction of penicillinase can liberate H^+, which can be monitored by the peak shift in the interference spectrum.

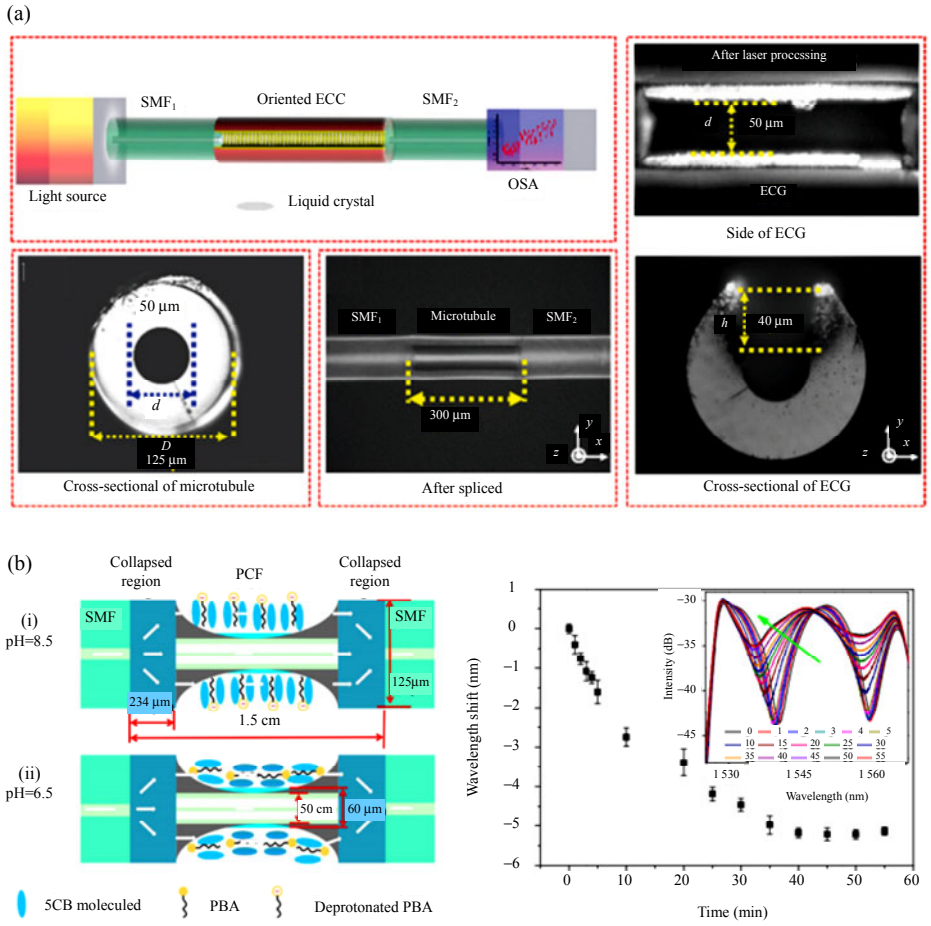

Fig. 10 LC-based MZI optical fiber sensing application: (a) schematic diagram of the LC-based fiber MZI and microscopic images of the local structure [24] and (b) schematic illustration of structural transition of the PBA-doped 5CB in the fiber MZI structure (left) and wavelength shift response to the enzymatic reactions between the PG and penicillinase (right) [25].

4.6 Others

Flow cytometry is a biological technique for counting and classifying microscopic particles that suspending in a fluid. This technique enables the continuous analysis of multiple parameters of individual cells as they travel through optical or electronic detectors. LC droplets are microscopic particles, and the orientational transition of the LC can impact the scattered light signal. Furthermore, flow cytometry can be used to statistically analyze a large number of LC droplets for reducing the individual differences. Miller *et al*. [163] employed flow cytometry to determine the internal ordering of LC droplets dispersed in the aqueous surfactant or phospholipid solutions. The adsorbate-induced variations in the LC droplet configuration cause unique alterations in the light scattering pattern. Radial droplets produce a narrower spread of side

scattering intensities than bipolar droplets. Furthermore, the scatter patterns for radial droplets have an "S-shape" property. Combining machine learning with flow cytometry to examine optical images of LCs allows for more accurate biological material categorization and identification. Jiang *et al*. [107] used flow cytometry data to train a convolutional neural network to predict endotoxin sources and concentrations directly from forward-scattering/side-scattering patterns.

Khan *et al*. [164] created LC-based biosensors using backscattering interferometry (BSI). An OTS coated square capillary loaded with 5CB is used in the sensor. The LC/aqueous interface in the capillary is functionalized with PAA-b-LCP, GO_x, and horseradish peroxidase for the glucose detection. Laser irradiation of the LC near the LC/aqueous interface results in backscattered fringes with the high contrast. The orientation of the LC affects the spatial position of the fringes, which modifies the photodetector's output voltage. Thus, an LOD for glucose as low as 0.008 mM with a linear range of 0.02 mM–9 mM is achieved. Yan *et al*. [165] presented a novel approach to quantify the concentration of the DMMP vapor. This method relies on the analysis of laser speckles captured by a 5CB film sensor. A linearly polarized laser beam is propagated through the LC film and subsequently directed onto a rough diffuser. A charge coupled device (CCD) is employed to capture speckle images from the LC and calculate the correlation coefficient, which is related to the orientation of the LC. The DMMP vapor is selectively detected over a 500 ppb to 5 ppm concentration range.

5. Conclusions

Several optical sensing technologies based on LC devices and their most recent research findings in the field of biochemistry are presented in this review. Polarizing microscopic imaging is the most prevalent method for detecting orientation changes induced by the specific recognition of biochemical molecules in NLC-based sensors. The reflectance spectroscopy is the most common optical detection method for CLC-based sensors, as the infiltration of the measured molecules alters the pitch of the CLC. Of course, there are some other optical sensing techniques that can be applied to both nematic and cholesteric LCs because they are based on the change in the refractive index of LCs brought by the biochemical molecular interactions, such as the WGM, SPR, optical fiber technology, and scattering technique. LC-based sensors offer several advantages in the applications, so they have gained increasing attention in recent years. Firstly, they eliminate the need for biomarkers, which simplifies the sensing process and lowers the cost of sensing. Secondly, the sensing devices are extremely convenient to manufacture, so they are accessible to a broad range of scientific researchers. Thirdly, LC sensing devices do not need the expensive detecting equipment, making them an economical option. Fourthly, the detection outcomes are intuitive and require no complex data processing. However, LC sensors also have their limitations, which will be the focus of the future research:

(1) LCs are fluid, and the fatal defect is their instability. Polymer dispersed LC, CLCP, and hydrogel-embedded LC can help to stabilize the LC, but the polymer or hydrogel can also interfere with the orientation of the LC. As a result, one of the future research topics will be the investigation of new ways to improve the stability of LCs.

(2) Non-reusability is also one of the weaknesses of LC sensors. Some CLC-based gas sensors are reusable, but a majority of biosensors used in solutions are not. The exploration of potential methods for reusing LC sensors remains an area that requires the further investigation.

(3) Enhancing the sensitivity of sensors to facilitate the detection of biological molecules at low concentrations is also an area of the future research. Some research employes nano-gold particles to enhance the sensitivity, however, the

literature on this topic is limited. Consequently, additional investigation into other methodologies is warranted.

(4) Every optical sensing method possesses its own set of advantages and disadvantages. At present, there has been a notable emphasis on polarizing microscopy as a sensing technology for NLC sensors and reflectance spectroscopy for CLC sensors, with less attention given to alternative sensing methods. The investigation and application of emerging optical sensing technologies in LC sensors is a prospective area for the future research.

(5) Currently, the majority of studies pertaining to LC sensors are limited to laboratory settings, with only a limited number of reports available on the development of portable LC sensor devices for practical applications. Furthermore, certain scholars engage in the development of microfluidic devices equipped with LC sensors for practical implementations. One of the prospective areas of the future research will be the practical application of LC sensors.

Scholars are increasingly interested in LC sensors. However, LC sensors are still in the field of research and need to be further investigated before they can be used in real-world environments.

Acknowledgment

This work was financially supported by the National Natural Science Foundation of China (Grant Nos. 62105125, 62075088, and 12174155); Natural Science Foundation of Guangdong Province (Grant No. 2022A1515140055); Research Fund of Guangdong-Hong Kong-Maco Joint Laboratory for Intelligent Micro-Nano Optoelectronic Technology (Grant No. 2020B1212030010); Guangdong Provincial Key Laboratory of Semiconductor Micro Display (Grant No. 2020B121202003); National Key Research and Development Program of China (Grant No. 2021YFB2800801); Natural Science Foundation of Guangdong Province for Distinguished Young Scholar (Grant No. 2020B1515020024); Key-Area Research and Development Program of Guangdong Province (Grant No. 2019B010138004); Guangdong Basic and Applied Basic Research Foundation (Grant No. 2021A1515110667); Special Project in Key Fields of the Higher Education Institutions of Guangdong Province (Grant No. 2020ZDZX3022).

Declarations

Conflict of Interest The authors declare that they have no competing interests.

Permissions All the included figures, tables, or text passages that have already been published elsewhere have obtained the permission from the copyright owner(s) for both the print and online format.

References

[1] J. L. Fergason, “Liquid crystals,” *Scientific American*, 1964, 211(2): 76–85.

[2] Y. Li, Z. Yin, and D. Luo, “Pre-compressed polymer cholesteric liquid crystal based optical fiber VOC sensor with high stability and a wide detection range,” *Optics Express*, 2022, 30(18): 32822–32832.

[3] M. K. Sadigh, P. Naziri, M. S. Zakerhamidi, A. Ranjkesh, and T. H. Yoon, “Temperature dependent features of polymer stabilized cholesteric liquid crystals based on selected liquid crystal characteristics,” *Optick*, 2021, 230(3): 166354.

[4] J. Hu, Y. Chen, Z. Ma, L. Zeng, D. Zhou, Z. Peng, *et al.*, “Temperature-compensated optical fiber sensor for volatile organic compound gas detection based on cholesteric liquid crystal,” *Optics Letters*, 2021, 46(14): 3324–3327.

[5] Y. Wang, Z. Ma, Z. Li, Y. Zhang, H. Zhang, G. Zheng, *et al.*, “Research on a novel temperature indicating device based on Bragg reflection waveguide of planar texture cholesteric liquid crystal layer,” *Molecular Crystals and Liquid Crystals*, 2022, 739(1): 78–87.

[6] V. K. Gupta, J. J. Skaife, T. B. Dubrovsky, and N. L. Abbott, “Optical amplification of ligand-receptor binding using liquid crystals,” *Science*, 1998, 279(3):

2077–2080.
[7] X. Zhan, Y. Liu, K. L. Yang, and D. Luo, "State-of-the-art development in liquid crystal biochemical sensors," *Biosensors*, 2022, 12(8): 577.
[8] J. Prakash, A. Parveen, Y. K. Mishra, and A. Kaushik, "Nanotechnology-assisted liquid crystals-based biosensors: towards fundamental to advanced applications," *Biosensors and Bioelectronics*, 2020, 168: 112562.
[9] S. A. Oladepo, "Development and application of liquid crystals as stimuli-responsive sensors," *Molecules*, 2022, 27(4): 1453.
[10] M. Khan, S. Liu, L. Qi, C. Ma, S. Munir, L. Yu, *et al.*, "Liquid crystal-based sensors for the detection of biomarkers at the aqueous/LC interface," *Trac-Trends in Analytical Chemistry*, 2021, 144: 116434.
[11] R. Xie, N. Li, Z. Li, J. Chen, K. Li, Q. He, *et al.*, "Liquid crystal droplet-based biosensors: promising for point-of-care testing," *Biosensors*, 2022, 12(9): 758.
[12] H. Wang, T. Xu, Y. Fu, Z. Wang, M. S. Leeson, J. Jiang, *et al.*, "Liquid crystal biosensors: principles, structure and applications," *Biosensors*, 2022, 12(8): 639.
[13] Z. An and C. Jang, "Simple and label-free liquid crystal-based optical sensor for highly sensitive and selective endotoxin detection by aptamer binding and separation," *Chemistryselect*, 2019, 4(4): 1416–1422.
[14] C. H. Chen, Y. C. Lin, H. H. Chang, and A. S. Y. Lee, "Ligand-doped liquid crystal sensor system for detecting mercuric ion in aqueous solutions," *Analytical* Chemistry, 2015, 87(8): 4546–4551.
[15] D. Das, S. Sidiq, and S. K. Pal, "Design of bio-molecular interfaces using liquid crystals demonstrating endotoxin interactions with bacterial cell wall components," *RSC Advances*, 2015, 5(81): 66476–66486.
[16] J. K. Gupta, J. S. Zimmerman, J. J. de Pablo, F. Caruso, and N. L. Abbott, "Characterization of adsorbate-induced ordering transitions of liquid crystals within monodisperse droplets," *Langmuir*, 2009, 25(16): 9016–9024.
[17] H. Zhang, Z. Miao, and W. Shen, "Development of polymer-dispersed liquid crystals: From mode innovation to applications," *Composites Part A*, 2022, 163: 107234.
[18] C. K. Chang, C. M. W. Bastiaansen, D. J. Broer, and H. L. Kuo, "Alcohol-responsive, hydrogen-bonded, cholesteric liquid-crystal networks," *Advanced Functional Materials*, 2012, 22(13): 2855–2859.
[19] C. K. Chang, C. W. M. Bastiaansen, D. J. Broer, and H. L. Kuo, "Discrimination of alcohol molecules using hydrogen-bridged cholesteric polymer networks," *Macromolecules*, 2012, 45(11): 4550–4555.
[20] X. Su, J. Xu, J. Zhang, C. Luan, and W. Huo, "Application progress of nano-signa amplification technology in liquid crystalbiosensor," *Chinese Journal of Analysis Laboratory*, 2019, 38(11): 1359–1365.
[21] C. K. Chang, H. L. Kuo, K. T. Tang, and S. W. Chiu, "Optical detection of organic vapors using cholesteric liquid crystals," *Applied Physics Letters*, 2011, 99(7): 073504.
[22] R. Duan, Y. Li, H. Li, and J. Yang, "Detection of heavy metal ions using whispering gallery mode lasing in functionalized liquid crystal microdroplets," *Biomedical Optics Express*, 2019, 10(12): 6073–6083.
[23] J. Tang, Z. Li, M. Xie, Y. Zhang, W. Long, S. Long, *et al.*, "Optical fiber bio-sensor for phospholipase using liquid crystal," *Biosensors and Bioelectronics*, 2020, 170: 112547.
[24] Y. Li, Y. Chen, D. Yi, Y. Du, W. Luo, X. Hong, *et al.*, "A self-assembled fiber Mach-Zehnder interferometer based on liquid crystals," *Journal of Materials Chemistry*, 2020, 8(32): 11153–11159.
[25] J. Hu, D. Fu, C. Xia, S. Long, C. Lu, W. Sun, *et al.*, "Fiber Mach-Zehnder-interferometer-based liquid crystal biosensor for detecting enzymatic reactions of penicillinase," *Applied Optics*, 2019, 58(17): 4806–4811.
[26] J. M. Brake, M. K. Daschner, Y. Y. Luk, and N. L. Abbott, "Biomolecular interactions at phospholipid-decorated surfaces ofliquidcrystals," *Science*, 2003, 302(5653): 2094–2097.
[27] D. K. Nguyen and C. H. Jang, "A cationic surfactant-decorated liquid crystal-based aptasensor for label-free detection of malathion pesticides in environmental samples," *Biosensors*, 2021, 11(3): 92.
[28] X. Niu, D. Luo, R. Chen, F. Wang, X. Sun, and H. Dai, "Optical biosensor based on liquid crystal droplets for detection of cholic acid," *Optics Communications*, 2016, 381: 286–291.
[29] P. Bao, D. A. Paterson, P. L. Harrison, K. Miller, S. Peyman, J. C. Jones, *et al.*, "Lipid coated liquid crystal droplets for the on-chip detection of antimicrobial peptides," *Lab on a Chip*, 2019, 19(6): 1082–1089.
[30] I. H. Lin, D. S. Miller, P. J. Bertics, C. J. Murphy, J. J. de Pablo, and N. L. Abbott, "Endotoxin-induced structural transformations in liquid crystalline droplets," *Science*, 2011, 332(6035): 1297–1300.
[31] C. G. Reyes, A. Sharma, and J. P. F. Lagerwall, "Non-electronic gas sensors from electrospun mats of liquid crystal core fibers for detecting volatile organic compounds at room temperature," *Liquid Crystals*, 2016, 43(13–15): 1986–2001.
[32] K. Schelski, C. G. Reyes, L. Pschyklenk, P. M. Kaul, and J. P. F. Lagerwall, "Quantitative volatile organic compound sensing with liquid crystal core fibers,"

Cell Reports Physical Science, 2021, 2(12): 100661.
[33] P. C. Wu, C. P. Pai, M. J. Lee, and W. Lee, "A single-substrate biosensor with spin-coated liquid crystal film for simple, sensitive and label-free protein detection," *Biosensors*, 2021, 11(10): 374.
[34] D. S. Millera and N. L. Abbott, "Influence of droplet size, pH and ionic strength on endotoxin-triggered ordering transitions in liquid crystalline droplets," *Soft Matter*, 2013, 9(2): 374–382.
[35] J. Y. Kwon, M. Khan, and S. Y. Park, "pH-responsive liquid crystal double emulsion droplets prepared using microfluidics," *RSC Advances*, 2016, 6(61): 55976–55983.
[36] G. Durey, Y. Ishii, and T. Lopez-Leon, "Temperature-driven anchoring transitions at liquid crystal/water interfaces," *Langmuir*, 2020, 36(32): 9368–9376.
[37] M. A. B. Pantoja and N. L. Abbott, "Surface-controlled orientational transitions in elastically strained films of liquid crystal that are triggered by vapors of toluene," *ACS Applied Materials & Interfaces*, 2016, 8(20): 13114–13122.
[38] H. J. Kim and C. H. Jang, "Liquid crystal-based capillary sensory platform for the detection of bile acids," *Chemistry and Physics of Lipids*, 2017, 204: 10–14.
[39] H. J. Kim and C. H. Jang, "Micro-capillary sensor for imaging trypsin activity using confined nematic liquid crystals," *Journal of Molecular Liquids*, 2016, 222: 596–600.
[40] T. K. H. Pham and C. H. Jang, "Simple, sensitive technique for α-amylase detection facilitated by liquid crystal-based microcapillary sensors," *Microchemical Journal*, 2021, 162: 105864.
[41] J. W. Huang, H. Hisamoto, and C. H. Chen, "Quantitative analysis of liquid crystal-based immunoassay using rectangular capillaries as sensing platform," *Optics Express*, 2019, 27(12): 17080–17090.
[42] X. Wang, E. Bukusoglu, and N. L. Abbott, "A practical guide to the preparation of liquid crystal-templated microparticles," *Chemistry of Materials*, 2017, 29(1): 53–61.
[43] V. Tomar, S. I. Hernandez, N. L. Abbott, J. P. Hernandez-Ortiz, and J. J. de Pablo, "Morphological transitions in liquid crystal nanodroplets," *Soft Matter*, 2012, 8(33): 8679–8689.
[44] D. K. Nguyen and C. H. Jang, "Simple and label-free detection of carboxylesterase and its inhibitors using a liquid crystal droplet sensing platform," *Micromachines*, 2022, 13(3): 490.
[45] J. Liu, T. Wang, J. Xiao, and L. Yu, "Portable liquid crystal droplet array in the capillary for rapid and sensitive detection of organophosphate nerve agents," *Microchemical Journal*, 2022, 178: 107334.
[46] F. Yin, S. Cheng , S. Liu, C. Ma, L. Wang, R. Zhao, *et al.*, "A portable digital optical kanamycin sensor developed by surface-anchored liquid crystal droplets," *Journal of Hazardous Materials*, 2021, 420: 126601.
[47] S. Cheng, M. Khan, F. Yin, C. Ma, J. Yuan, T. Jiang, *et al.*, "Surface-anchored liquid crystal droplets for the semi-quantitative detection of aflatoxin B1 in food samples," *Food Chemistry*, 2022, 390: 133202.
[48] S. Xie, R. He, Q. Zhu, M. Jin, R. Yang, S. Shen, *et al.*, "Label-free optical sensor based on liquid crystal sessile droplet array for penicillin G determination," *Colloids and Surface A*: *Physicochemical and Engineering Aspects*, 2022, 644: 128728.
[49] J. K. Gupta, J. S. Zimmerman, J. J. de Pablo, F. Caruso, and N. L. Abbott, "Characterization of adsorbate-induced ordering transitions of liquid crystals within monodisperse droplets," *Langmuir*, 2009, 25(16): 9016–9024.
[50] J. Deng, D. Han, and J. Yang, "Applications of microfluidics in liquid crystal-based biosensors," *Biosensors*, 2021, 11(10): 385.
[51] O. H. Piñeres-Quiñones, D. M. Lynn, and C. Acevedo-Vélez, "Environmentally responsive emulsions of thermotropic liquid crystals with exceptional long-term stability and enhanced sensitivity to aqueous amphiphiles," *Langmuir*, 2022, 38(3): 957–967.
[52] J. Deng, X. Wang, W. Liang, D. Richardsonb, Q. Luc, and J. Fang, "Surface modified liquid crystal droplets as an optical probe for the detection of bile acids in microfluidic channels," *Colloids and Surfaces A-Physicochemical and Engineering Aspects*, 2018, 542: 52–58.
[53] G. Zhang, A. Zhu, S. Wang, Q. Chen, B. Liu, J. Zhou, *et al.*, "Stabilizing liquid crystal droplets with hydrogel films and its application in monitoring adenosine triphosphate," *Colloids and Surfaces A: Physicochemical and Engineering Aspects*, 2022, 654: 130122.
[54] Z. Ma, J. Sun, S. Zhou, W. Shan, Y. Yan, and Y. Liu, "Compact fiber sensor for pH measurement based on the composite effect of hydrogel deformation and LC refractive index variation," *Optics Letters*, 2023, 48(1): 139–142.
[55] L. Liu, W. Li, X. Wang, Y. Xie, Y. Li, and Z. Wu, "Functional liquid crystal core/hydrogel shell microcapsules for monitoring live cells in a 3D microenvironment," *Analytical Chemistry*, 2023, 95(5): 2750–2756.
[56] L. L. Teresa and F. N. Alberto, "Drops and shells of liquid crystal," *Colloid Polymer Science*, 2011, 289(4): 345–359.
[57] I. S. Heo and S. Y. Park, "Smart shell membrane prepared by microfluidics with reactive nematic liquid crystal mixture," *Sensors and Actuators B–Chemical*, 2017, 251: 658–666.
[58] J. Wang, A. Jákli, and J. L. West, "Liquid crystal/

polymer fiber mats as sensitive chemical sensors," *Journal of Molecular Liquids*, 2018, 267: 490–495.

[59] S. R. Kim, R. R. Shah, and N. L. Abbott, "Orientations of liquid crystals on mechanically rubbed films of bovine serum albumin: a possible substrate for biomolecular assays based on liquid crystals," *Analytical Chemistry*, 2000, 72(19): 4646–4653.

[60] R. R. Shah and N. L. Abbott, "Principles for measurement of chemical exposure based on recognition-driven anchoring transitions in liquid crystals,"*Science*, 2001, 293(5533): 1296–1299.

[61] M. Škarabot, E. Osmanagič, and I. Muševič, "Surface anchoring of nematic liquid crystal 80CB on a DMOAP-silanated glass surface," *Liquid Crystals*, 2006, 33(5): 581–585.

[62] H. Lin, L. Ke, H. C. Liang, and W. Kuo, "Tunable pretilt angle based on gelator-doped planar liquid crystal cells," *Liquid Crystals*, 2021, 48: 1448–1456.

[63] T. K. Chang, M. J. Lee, and W. Lee, "Quantitative biosensing based on a liquid crystal marginally aligned by the PVA/DMOAP composite for optical signal amplification," *Biosensors*, 2022, 12(4): 218.

[64] M. J. Lee, F. F. Duan, P. C. Wu, and L. Wei, "Liquid crystal-photopolymer composite films for label-free single-substrate protein quantitation and immunoassay," *Biomedical Optics Express*, 2020, 11(9): 4915–4927.

[65] T. K. Chang, P. C. Tung, M. J. Lee, and W. Lee, "A liquid-crystal aptasensing platform for label-free detection of a single circulating tumor cell," *Biosensors and Bioelectronics*, 2022, 216: 114607.

[66] X. Niu, Y. Liu, F. Wang, and D. Luo, "Highly sensitive and selective optical sensor for lead ion detection based on liquid crystal decorated with DNAzyme," *Optics Express*, 2019, 27(21): 30421–30428.

[67] Z. Khoshbin, H. Zahraee, J. Zamanian, A. Verdian, M. Ramezani, M. Alibolandi, *et al.*, "A label-free liquid crystal-assisted aptasensor for trace level detection of tobramycin in milk and chicken egg samples,"*Analytica Chimica Acta*, 2022, 1236(15): 340588.

[68] M. L. Bungabong, P. B. Ong, and K. L. Yang, "Using copper perchlorate doped liquid crystals for the detection of organophosphonate vapor," *Sensors and Actuators B–Chemical*, 2010, 148(2): 420–426.

[69] G. Li, B. Gao, M. Yang, L. C. Chen, and X. L. Xiong, "Homeotropic orientation behavior of nematic liquid crystals induced by copper ions," *Colloids and Surfaces B–Biointerfaces*, 2015, 130: 287–291.

[70] K. L. Yang, K. Cadwell, and N. L. Abbott, "Use of self-assembled monolayers, metal ions and smectic liquid crystals to detect organophosphonates," *Sensors and Actuators B–Chemical*, 2005, 104(1): 50–56.

[71] J. M. Brake, A. D. Mezera, and N. L. Abbott, "Effect of surfactant structure on the orientation of liquid crystals at aqueous-liquid crystal interfaces," *Langmuir*, 2003, 19(16): 6436–6442.

[72] S. Lu, Y. Guo, L. Qi, Q. Hu, and L. Yu, "Highly sensitive and label-free detection of catalase by a H_2O_2-responsive liquid crystal sensing platform," *Sensors and Actuators B–Chemical*, 2021, 344: 130279.

[73] L. Zhou, Q. Kang, and M. Fang, "Label-free, rapid, and sensitive detection of carboxylesterase using surfactant-doped liquid crystal sensor," *Journal of Molecular Liquids*, 2019, 296: 111921.

[74] M. Devi, I. Verma, and S. K. Pal, "Distinct interfacial ordering of liquid crystals observed by protein-lipid interactions that enabled the label-free sensing of cytoplasmic protein at the liquid crystal-aqueous interface," *Analyst*, 2021, 146(23): 7152–7159.

[75] I. Verma, S. Sidiq, and S. K. Pal, "Protein triggered ordering transitions in poly (L-lysine)-coated liquid crystal emulsion droplets," *Liquid Crystals*, 2019, 46(9): 1318–1326.

[76] X. Yang and Z. Yang, "Simple and rapid detection of ibuprofen-a typical pharmaceuticals and personal care products – by a liquid crystal aptasensor," *Langmuir*, 2022, 38(1): 282–288.

[77] A. D. Price and D. K. Schwartz. "DNA hybridization-induced reorientation of liquid crystal anchoring at the nematic liquid crystal/aqueous interface," *Journal of the American Chemical Society*, 2008, 130(26): 8188–8194.

[78] M. Khan, A. R. Khan, J. H. Shin, and S. Y. Park, "A liquid-crystal based DNA biosensor for pathogen detection ion," *Scientific Reports*, 2016, 6: 22676.

[79] Y. Wang, Q. Hu, Y. Guo, and L. Yu, "A cationic surfactant-decorated liquid crystal sensing platform for simple and sensitive detection of acetylcholinesterase and its inhibitor," *Biosensors & Bioelectronics*, 2015, 72: 25–30.

[80] H. Ma, S. Lu, Q. Xie, T. Wang, H. Lu, and L.Yu,"A stable liquid crystals sensing platform decorated with cationic surfactant for detecting thrombin," *Microchemical Journal*, 2021, 170: 106698.

[81] J. Ping, L. Qi, Q. Wang, S. Liu, Y. Jiang, L. Yu, *et al.*, "An integrated liquid crystal sensing device assisted by the surfactant-embedded smart hydrogel," *Biosensors & Bioelectronics*, 2021, 187: 113313.

[82] H. Ma, Q. Kang, T. Wang, and L. Yu, "A liquid crystals-based sensing platform for detection of α-amylase coupled with destruction of host-guest interaction," *Colloids and Surfaces B–Biointerfaces*, 2019, 173: 616-622.

[83] K. N. Duy and C. H. Jang, "A label-free liquid crystal biosensor based on specific DNA aptamer probes for sensitive detection of amoxicillin antibiotic," *Micromachines*, 2021, 12(4): 370.

[84] Y. Wang, B. Wang, X. Xiong, and S. Deng, "A self-oriented beacon liquid crystal assay for kanamycin detection with AuNPs signal enhancement," *Analytical Methods*, 2022, 14(4): 410–416.

[85] Q. Z. Hu and C. H. Jang, "Using liquid crystals for the real-time detection of urease at aqueous/liquid crystal interfaces," *Journal of Materials Science*, 2012, 47(2): 969–975.

[86] Y. Wang, L. Zhao, A. Xu, L. Wang, L. Zhang, S. Liu, *et al.*, "Detecting enzymatic reactions in penicillinase via liquid crystal microdroplet-based pH sensor," *Sensors and Actuators B–Chemical*, 2018, 258: 1090–1098.

[87] X. Bi, D. Hartono, and K. L. Yang, "Real-time liquid crystal pH sensor for monitoring enzymatic activities of penicillinase," *Advanced Functional Materials*, 2009, 19(23): 3760–3765.

[88] M. Sundas, I. K. Kang, and S. Y.Park, "Polyelectrolytes functionalized nematic liquid crystal-based biosensors: an overview," *Trends in Analytical Chemistry*, 2016, 83: 80–94.

[89] T. Bera and J. Fang, "Polyelectrolyte-coated liquid crystal droplets for detecting charged macromolecules," *Journal Materials Chemistry*, 2012, 22(14): 6807–6812.

[90] D. H. Yeo and S. Y. Park, "Liquid-crystal-based biosensor for detecting Ca^{2+} in human saliva," *Journal of Industrial and Engineering Chemistry*, 2019, 74: 193–198.

[91] M. Khan and S. Y. Park, "Specific detection of avidin-biotin binding using liquid crystal droplets," *Colloids and Surfaces B–Biointerfaces*, 2015, 127: 241–246.

[92] C. S. Park, K. Iwabata, U. Sridhar, M. Tsuei, K. Singh, Y. K. Kim, *et al.*, "A new strategy for reporting specific protein binding events at aqueous-liquid crystal interfaces in the presence of non-specific proteins," *ACS Applied Materials Interfaces*, 2020, 12(7): 7869–7878.

[93] Y. S. Choi, Y. J. Lee, H. J. Kwon, and S. D. Lee, "Optical detection of the ligand-receptor binding by anchoring transitions of liquid crystals," *Materials Science and Engineering: C*, 2004, 24(1–2): 237–240.

[94] N. A. Lockwood, J. K. Gupta, and N. L. Abbott, "Self-assembly of amphiphiles, polymers and proteins at interfaces between thermotropic liquid crystals and aqueous phases," *Surface Science Reports*, 2008, 63(6): 255–293.

[95] N. A. Lockwood and N. L. Abbott, "Self-assembly of surfactants and phospholipids at interfaces between aqueous phases and thermotropic liquid crystals," *Current Opinion in Colloid & Interface Science*, 2005, 10(2–3): 111–120.

[96] X. Wang, *Crystal Optics.* Nanjing: Nanjing University Press, 2014.

[97] J. M. Brake, M. K. Daschner, and N. L. Abbott, "Formation and characterization of phospholipid monolayers spontaneously assembled at interfaces between aqueous phases and thermotropic liquid crystals," *Langmuir*, 2005, 21(6): 2218–2228.

[98] X. Su, J. Xu, J. Zhang, D. Yang, W. Huo, and C. He, "Detection of Cecropin B by liquid-crystal biosensor based on AuNPs signal amplification," *Liquid Crystals*, 2020, 47(12): 1794–1802.

[99] H. Liu, X. Su, J. Zhang, J. Xu, D. Yang, and Q. Chen, "Highly sensitive and rapid detection of protein kinase C based on liquid crystal biosensor," *Colloids and Surfaces A–Physicochemical and Engineering Aspects*, 2021, 628: 127346.

[100] L. Qi, S. Liu, Y. Jiang, J. Lin, L. Yu, and Q. Hu, "Simultaneous detection of multiple tumor markers in blood by functional liquid crystal sensors assisted with target-induced dissociation of aptamer," *Analytical Chemistry*, 2020, 92(5): 3867–3873.

[101] S. Cheng, M. Khan, F. Yin, W. Wu, T. Sun, Q. Hu, *et al.*, "Liquid crystal-based sensitive and selective detection of uric acid and uricase in body fluids," *Talanta*, 2022, 244: 123455.

[102] N. Majeed, A. Noor, and H. M. Siddiqi, "Non-enzymatic liquid crystal-based detection of copper ions in water," *Chemistry Select*, 2023, 8(3): e202204433.

[103] M. G. Shemirani, F. Habibimoghaddam, M. Mohammadimasoudi, M. Esmailpour, and A. Goudarzi, "Rapid and label-free methanol identification in alcoholic beverages utilizing a textile grid impregnated with chiral nematic liquid crystals," *ACS Omega*, 2022, 7(42): 37546–37554.

[104] Y. Zhou, E. Bukusoglu, J. A. Martínez-Gonzalez, M. Rahimi, T. F. Roberts, R. Zhang, *et al.*, "Structural transitions in cholesteric liquid crystal droplets," *ACS Nano*, 2016, 10(7): 6484–6490.

[105] H. G. Lee, S. Munir, and S. Y. Park, "Cholesteric liquid crystal droplets for biosensors," *ACS Applied Materials Interfaces*, 2016, 8(39): 26407–26417.

[106] B. Gollapelli, A. K. Tatipamula, S. Dewanjee, R. S. Pathintia, and J. Vallamkondu, "Detection of bile acids using optical biosensors based on cholesteric liquid crystal droplets," *Journal of Materials Chemistry C*, 2021, 9(39): 13991–14002.

[107] S. Jiang, J. Noh, C. Park, A. D. Smith, N. L. Abbott, and V. M. Zavala, "Using machine learning and liquid crystal droplets to identify and quantify endotoxins from different bacterial species," *Analyst*, 2021, 146(4): 1224–1233.

[108] Y. Zhang, S. Xu, R. Zhang, Z. Deng, Y. Liu, J. Tian, *et al.*, "Automated calculation of liquid crystal sensing images based on deep learning," *Analytical Chemistry*, 2022, 94(37): 127810–12787.

[109] N. Bao, S. Jiang, A. Smith, J. J. Schauer, M.

Mavrikakis, R. C. Van Lehn, *et al.*, "Sensing gas mixtures by analyzing the spatiotemporal optical responses of liquid crystals using 3D convolutional neural networks," *ACS Sensors*, 2022, 7(9): 2545–2555.

[110] M. Esmailpour, M. Mohammadimasoudi, M. G. Shemirani, A. Goudarzi, M. H. Heidari Beni, H. Shahsavarani, *et al.*, "Rapid, label-free and low-cost diagnostic kit for COVID-19 based on liquid crystals and machine learning," *Biosensors and Bioelectronics:X*, 2022, 12: 100233.

[111] J. Frazão, S. Palma, H. M. A. Costa, C. Alves, A. C. A. Roque, and M. Silveira, "Optical gas sensing with liquid crystal droplets and convolutional neural networks," *Sensors*, 2021, 21(8): 2854.

[112] Y. Cao, H. Yu, N. L. Abbott, and V. M. Zavala, "Machine learning algorithms for liquid crystal-based sensors," *ACS Sensors*, 2018, 3(11): 2237–2245.

[113] A. D. Smith, N. Abbott, and V. M. Zavala, "Convolutional network analysis of optical micrographs for liquid crystal sensors," *Journal of Physical Chemistry C*, 2020, 124(28): 15152–15161.

[114] L. Qi, Q. Hu, Q. Kang, Y. Bi, Y. Jiang, and L. Yu, "Detection of biomarkers in blood using liquid crystals assisted with aptamer-target recognition triggered in situ rolling circle amplification on magnetic beads," *Analytical Chemistry*, 2019, 91(18): 11653–11660.

[115] J. Liu, Q. Hu, L. Qi, J. M. Lin, and L. Yu, "Liquid crystal-based sensing platform for detection of Pb^{2+} assisted by DNAzyme and rolling circle amplification," *Journal of Hazardous Materials*, 2020, 400: 123218.

[116] L. Zhao, Y. Wang, Y. Yuan, Y. Liu, S. Liu, W. Sun, *et al.*, "Whispering gallery mode laser based on cholesteric liquid crystal microdroplets as temperature sensor," *Optics Communications*, 2017, 402: 181–185.

[117] D. Zhou, Z. Lan, W. Cao, Y. Chen, S. Zhang, J. Hu, *et al.*, "Liquid crystal optical fiber sensor based on misaligned core configuration for temperature and mixed volatile organic compound detection," *Optics and Laser Technology*, 2022, 156: 108545.

[118] D. I. Avsar and E. Bukusoglu, "Chameleon skin-inspired polymeric particles for the detection of toluene vapor," *Soft Matter*, 2020, 16(37): 8683–8691.

[119] K. J. Kek, J. J. Z. Lee, Y. Otono, and S. Ishihara, "Chemical gas sensors using chiral nematic liquid crystals and its applications," *Journal of the Society for Information Display*, 2017, 25(6): 366–373.

[120] L. Sutarlie, J. Y. Lim, and K. L. Yang, "Cholesteric liquid crystals doped with dodecylamine for detecting aldehyde vapors," *Analytical Chemistry*, 2011, 83(13): 5253–5258.

[121] L. Sutarlie, H. Qin, and K. L. Yang, "Polymer stabilized cholesteric liquid crystal arrays for detecting vaporous amines," *Analyst*, 2010, 135(7): 1691–1696.

[122] T. Y. Yeh, M. F. Liu, R. D. Lin, and S. J. Hwang, "Alcohol selective optical sensor based on porous cholesteric liquid crystal polymer networks," *Molecules*, 2022, 27(3): 773.

[123] M. Moirangthem, R. Arts, M. Merkx, and A. P. H. J. Schenning, "An optical sensor based on a photonic polymer film to detect calcium in serum," *Advanced Functional Materials*, 2016, 26(8): 1154–1160.

[124] J. E. Stumpel, E. R. Gil, A. B. Spoelstra, C. W. M. Bastiaansen, B. D. J. Schenning, and A. P. H. J. Schenning, "Stimuli-responsive materials based on interpenetrating polymer liquid crystal hydrogels," *Advanced Functional Materials*, 2015, 25(22): 3314–3320.

[125] K. G. Noh and S. Y. Park, "Biosensor array of interpenetrating polymer network with photonic film templated from reactive cholesteric liquid crystal and enzyme-immobilized hydrogel polymer," *Advanced Functional Materials*, 2018, 28(22): 1707562.

[126] J. S. Lim, Y. J. Kim, and S. Y. Park, "Functional solid-state photonic droplets with interpenetrating polymer network and their applications to biosensors," *Sensors and Actuators B–Chemical*, 2021, 329: 129165.

[127] Y. Yang, D. Zhou, X. Liu, Y. Liu, S. Liu, P. Miao, *et al.*, "Optical fiber sensor based on a cholesteric liquid crystal film for mixed VOC sensing," *Optics Express*, 2020, 28,(21): 31872–31881.

[128] Y. Su, Z. Lan, J. Wang, L. Zeng, D. Zhou, Z. Peng, *et al.*, "Optical fiber sensor for determination of methanol ratio in methanol-doped ethanol based on two cholesteric liquid crystal droplets embedded in chitosan," *Journal of Lightwave Technology*, 2021, 39(15): 5170–5176.

[129] K. D. Cadwell, M. E. Alf, and N. L. Abbott, "Infrared spectroscopy of competitive interactions between liquid crystals, metal salts, and dimethyl methylphosphonate at surfaces," *Journal of Physical Chemistry B*, 2006, 110(51): 26081–26088.

[130] Y. Zhang, Q. Song, D. Zhao, X. Tang, Y. Zhang, Z. Liu, *et al.*, "Review of different coupling methods with whispering gallery mode resonator cavities for sensing," *Optics and Laser Technology*, 2023, 159: 108955.

[131] Z. Wang, Y. Zhang, X. Gong, Z. Yuan, S. Feng, T. Xu, *et al.*, "Bio-electrostatic sensitive droplet lasers for molecular detection," *Nanoscale Advances*, 2020, 2(7): 2713–2719.

[132] M. Humar and I. Muševič, "Surfactant sensing based on whispering-gallery-mode lasing in

liquid-crystal microdroplets," *Optics Express*, 2011, 19(21): 19836–19844.
[133] R. Duan, Y. Li, H. Li, and J. Yang, "Real-time monitoring of the enzymatic reaction of urease by using whispering gallery mode lasing," *Optics Express*, 2019, 27(24): 35427–35436.
[134] R. Duan, Y. Li, B. Shi, H. Li, and J. Yang, "Real-time, quantitative and sensitive detection of urea by whispering gallery mode lasing in liquid crystal microdroplet," *Talanta*, 2020, 209: 120513.
[135] R. Duan, X. Hao, Y. Li, and H. Li, "Detection of acetylcholinesterase and its inhibitors by liquid crystal biosensor based on whispering gallery mode," *Sensors and Actuators B–Chemical*, 2020, 308: 127672.
[136] Z. Ma, M. Xu, S. Zhou, W. Shan, D. Zhou, Y. Yan, *et al.*, "Ultra-low sample consumption consecutive-detection method for biochemical molecules based on a whispering gallery mode with a liquid crystal microdroplet," *Optics Letters*, 2022, 47(2): 381–384.
[137] R. Duan, Y. Li, Y. He, Y. Yuan, and H. Li, "Quantitative and sensitive detection of lipase using a liquid crystal microfiber biosensor based on the whispering-gallery mode," *Analyst*, 2020, 145(23): 7595–7602.
[138] R. Duan, Y. Li, Y. Yuan, L. Liu, and H. Li, "Functionalised liquid crystal microfibers for hydrogen peroxide and catalase detection using whispering gallery mode," *Liquid Crystals*, 2020, 47(11): 1708–1717.
[139] Z. Wang, Y. Liu, C. Gong, Z. Yuan, L. Shen, P. Chang, *et al.*, "Liquid crystal-amplified optofluidic biosensor for ultra-highly sensitive and stable protein assay", *PhotoniX*, 2021, 2(1): 1–16.
[140] R. W. Wood, "On a remarkable case of uneven distribution of light in a diffraction grating," *Philosophical Magazine*, 1902, 4(19–24): 396–402.
[141] A. Otto, "Excitation of nonradiative surface plasma waves in silver by the method of frustrated total reflection," *Zeitschrift für Physik*, 1968, 216(4): 398–410.
[142] E. Kretschmann, "Die bestimmung optischer konstanten von metallen durch anregung von oberflächenplasmaschwingungen," *Zeitschrift für Physik a Hadrons and nuclei*, 1971, 241(4): 313–324.
[143] Y. Zhao, R. Tong, F. Xia, and Y. Peng, "Current status of optical fiber biosensor based on surface plasmon resonance", *Biosensors and Bioelectronics*, 2019, 142: 111505.
[144] A. K. Singh, M. Anwar, R. Pradhan, M. S. Ashar, N. Rai, and S. Dey, "Surface plasmon resonance based-optical biosensor: emerging diagnostic tool for early detection of diseases," *Journal of Biophotonics*, 2023, 16(7): 202200380.
[145] S. Das, R. Devireddy, and M. R. Gartia, "Surface plasmon resonance (SPR) sensor for cancer biomarker detection," *Biosensors*, 2023, 13(3): 396.
[146] A. Vahedi and M. Kouhi, "Liquid crystal-based surface plasmon resonance biosensor," *Plasmonics*, 2020, 15(1): 61–71.
[147] A. S. A. Abuabed, "Study of the effect of nematic order degradation in liquid crystal-based surface plasmon resonance sensors," *Photonics*, 2017, 4(2): 24.
[148] A. Vahedi and M. Kouhi, "Temperature effects on liquid crystal-based tunable biosensors," *Optik*, 2021, 242: 167383.
[149] N. Mehan, "Effects of optic axis rotation on the sensing properties of nematic liquid crystal based surface plasmon resonance (SPR) sensor," *Optical Materials*, 2023, 136: 113472.
[150] B. Kieser, D. Pauluth, and G. Gauglitz, "Nematic liquid crystals as sensitive layers for surface plasmon resonance sensors," *Analytica Chimica Acta*, 2001, 434(2): 231–237.
[151] G. M. Koenig Jr, B. T. Gettelfinger, J. J. de Pablo, and N. L. Abbott, "Using localized surface plasmon resonances to probe the nanoscopic origins of adsorbate-driven ordering transitions of liquid crystals in contact with chemically functionalized gold nanodots," *Nano Letters*, 2008, 8(8): 2362–2368.
[152] F. Esposito, A. Srivastava, L. Sansone, M. Giordano, S. Campopiano, and A. Iadicicco, "Label-free biosensors based on long period fiber gratings: a review," *IEEE Sensors Journal*, 2021, 21(11): 12692–12705.
[153] J. Zhou, Q. Qi, C. Wang, Y. Qian, G. Liu, Y. Wang, *et al.*, "Surface plasmon resonance (SPR) biosensors for food allergen detection in food matrices," *Biosensors and Bioelectronics*, 2019, 142: 111449.
[154] C. Liu, H. Chen, Q. Chen, Z. Gao, B. Wu, X. Fan, *et al.*, "Sagnac interferometer-based optical fiber strain sensor with exceeding free spectral measurement range and high sensitivity," *Optics and Laser Technology*, 2023, 159: 108935.
[155] P. Nag, K. Sadani, S. Mohapatra, S. Mukherji, and S. Mukherji, "Evanescent wave optical fiber sensors using enzymatic hydrolysis on nanostructured polyaniline for detection of β-lactam antibiotics in food and environment," *Analytical Chemistry*, 2021, 93(4): 2299–2308.
[156] H. Deng, X. Chen, Z. Huang, S. Kang, W. Zhang, H. Li, *et al.*, "Optical fiber based Mach-Zehnder interferometer for APES detection," *Sensors*, 2021, 21(17): 5870.
[157] S. Tang, M. Zou, C. Zhao, Y. Jiang, R. Chen, Z. Xu, *et al.*, "Fabry-Perot interferometer based on a fiber-tip fixed supported bridge for fast glucose concentration measurement," *Biosensors*, 2022, 12(6): 391.

[158] R. Wang, M. Yan, M. Jiang, Y. Li, X. Kang, M. Hu, *et al.*, "Label-free and selective cholesterol detection based on multilayer functional structure coated fiber Fabry-Perot interferometer probe," *Analytica Chimica Acta*, 2023, 1252: 341051.

[159] V. Vikas and P. Saccomandi, "Design considerations of an ITO-coated U-shaped fiber optic LMR biosensor for the detection of antibiotic ciprofloxacin," *Biosensors*, 2023, 13(3): 362.

[160] N. L. N. Tran, B. T. Phan, H. K. T. Ta, T. T. K. Chi, B. T. T. Hien, N. T. T. Phuong, *et al.*, "Gold nanoparticles are capped under the IRMOF-3 platform for in-situ surface-enhanced Raman scattering technique and optic fiber sensor," *Sensors and Actuators A–Physical*, 2022, 347: 113932.

[161] T. Y. Ho, J. W. Huang, B. C. Peng, W. C. Tsao, and C. H. Chen, "Liquid crystal-based sensor system for detecting formaldehyde in aqueous solutions," *Microchemical Journal*, 2020, 158: 105235.

[162] J. Tang, J. Fang, Y. Liang, B. Zhang, Y. Luo, X. Liu, *et al.*, "All-fiber-optic VOC gas sensor based on side-polished fiber wavelength selectively coupled with cholesteric liquid crystal film," *Sensors and Actuators B–Chemical*, 2018, 273: 1816–1826.

[163] D. S. Miller, X. Wang, J. Buchen, O. D. Lavrentovich, and N. L. Abbott, "Analysis of the internal configurations of droplets of liquid crystal using flow cytometry," *Analytical Chemistry*, 2013, 85(21): 10296–10303.

[164] M. Khan and S. Y. Park, "Liquid crystal-based biosensor with backscattering interferometry: a quantitative approach," *Biosensors and Bioelectronics*, 2017, 87: 976–983.

[165] Y. Yan, N. Bu, X. Bai, M. Wang, Y. Ma, S. Jia, *et al.*, "A liquid crystal optical sensor for simple and quantitative determination of dimethylmethylphosphonate using laser speckle," *Optics and Laser in Engineering*, 2023, 170: 107763.